A lumped plasticity model for corrosion damaged reinforced concrete columns

Text written date: 04/12/2021

Revised date: 29/10/2021

Author 1

- Hamed Roohbakhsh, PhD Candidate
- Structural Engineering Research Center, International Institute of Earthquake Engineering and Seismology, Tehran, Iran
- https://orcid.org/0000-0002-0000-3733

Author 2 **(corresponding author)**

- Afshin Kalantari, Associate Professor
- Structural Engineering Research Center, International Institute of Earthquake Engineering and Seismology, Tehran, Iran

Author 3

- Mohammad M. Kashani, Associate Professor
- University of Southampton, Southampton, UK
- https://orcid.org/0000-0003-0008-0007

Author 4

- Akanshu Sharma, Junior-Professor
- Institute of Construction Materials, University of Stuttgart, Stuttgart, Germany
- https://orcid.org/0000-0001-5426-1829

contact details of corresponding author:

Associate Professor, Structural Engineering Research Centre, International Institute of Earthquake Engineering and Seismology, Tehran 19537-14453, Iran. Email: a.kalantari@iiees.ac.ir

Accepted Manuscript

Abstract

Chloride-induced corrosion is one of the most important reasons for the strength degradation of reinforced concrete (RC) bridges. As the piers of RC bridges are important element to sustain lateral loads, corrosion of columns in pier may lead to significant degradation. So it is necessary to have an appropriate evaluation technique to assess the effect of corrosion on the RC columns behaviour. numerical modelling approaches which are based on the concentrated plastic hinge can predict structural behaviour rapidly and with acceptable accuracy which are highly regarded by engineers. In this study, a numerical approach is conducted to develop an empirical lumped plasticity model for corroded RC column elements. 13440 RC column specimens, including corroded and uncorroded, rectangular, and circular cross sections are analysed under monotonic and cyclic loading. Lumped plasticity model is extracted based on the regression of the cyclic and monotonic analysis results. Finally, calibrated model is verified through experimental and out-of-parametric study models with high accuracy. The new developed plastic hinge model can be used to model and analyse corroded bridge columns rapidly. The result can be appropriate to be employed for modelling in the further assessment such as fragility analysis or rehabilitation.

Keywords

Corrosion; bridges; concrete structures

Accepted Manuscript

List of notations

ψ is the corrosion damage rate of longitudinal bars (mass loss ratio in percentage)

υ is the axial load ratio ($^{P}/_{A_g f_c'}$)

P unfactored axial load, kN

A_g is the cross section gross area, mm^2

d is the cross section effective depth, mm

ρ_v is the longitudinal bar ratio

f_c' is the concrete compressive strength, MPa

f_y is the longitudinal reinforcement yield strength, MPa

f_{yh} is the transvers reinforcement yield strength, MPa

ρ_h is the transvers bar volumetric ratio

L_{eff} is the effective buckling length of longitudinal bars, mm

f_u is the longitudinal reinforcement ultimate strength, MPa

M_y is the yield moment in plastic hinge model, MPa

θ_y is the yield rotation in plastic hinge model

M_p is the capping moment in plastic hinge model, MPa

θ_p is the capping rotation in plastic hinge model

θ_{pc} is the post-capping rotation in plastic hinge model

Accepted Manuscript

1. Introduction

Corrosion of reinforcement in RC bridges is the most important durability problem which is not considered directly in the design procedure (Parke & Hewson, 2008). Several parameters such as temperature around RC bridge, clear cover thickness and humidity would affect the corrosion rate in the RC member (Tuutti, 1982). The chloride ion around RC bridge acts as a catalyst in the corrosion of reinforcement. This material doesn't consume in corrosion process and usually leads to pitting corrosion. (The Institution of Structural Engineers, 2010). Corrosion in the RC member decreases the yield strength of reinforcing steel bars and bars cross section (Du et al., 2005). Previous studies have shown that corrosion in the RC member can affect mechanical behaviour of steel bars such as low-cyclic fatigue and inelastic buckling significantly (Kashani, et al., 2013; Kashani, et al., 2014; Ge, et al., 2020 (b); Ge, et al., 2020 (a)) Concrete cover cracking and spalling (Du, et al., 2005 (a)) and reduction in bonding strength between bars and concrete (Lundgren, 2007) are another result of corrosion in reinforced concrete structures. Due to mentioned corrosion effects, a significant strength degradation occurs in the RC structures as a result of corrosion (Ge, et al., 2020 (b); Ge, et al., 2020 (a); Roohbakhsh & Kalantari, 2018).

RC bridges are important infrastructures which have significant role in in transportation. As shown in Figure 1, each RC bridge may have several piers and each of the piers contains one or more RC columns. Bridge piers have important role in association with all other bridge supports such as abutments to sustain seismic loads. Therefore, corrosion of columns of bridge piers can affect its resistance against lateral loads such as earthquake (Ge, et al., 2020 (a); Ge, et al., 2020 (b)). Recent experimental and numerical studies on the effect of corrosion on seismic performance and nonlinear behaviour of RC columns have shown that corrosion has significantly increased seismic vulnerability of such structural components (Cardone, et al., 2013; Afsar Dizaj, et al., 2018; Chang, et al., 2020; Meda, et al., 2014; Yang, et al., 2016; Li, et al., 2020; Yang, et al., 2020; Yu, et al., 2020). Numerous numerical modelling has been proposed by previous researchers in the literature to consider the effect of corrosion in RC members. However some of these finite element models are based on degradation of steel bars properties like cross section and yield strength (Alipour, et al., 2011; Rao, et al., 2017), while a few of recent studies have considered new modelling procedure to contribute almost all aspect of corrosion on the RC

Accepted Manuscript

member (Taucer, et al., 1991; Clough & Benuska, 1967; Takizawa, 1976). Unlike other studies, in such finite element modelling, the effect of corrosion on the low-cyclic fatigue and inelastic buckling of longitudinal bars have been considered.

Nonlinear behaviour in FE modelling of RC members can be conducted in two ways. Distributed plasticity and lumped plasticity (Giberson, 1967). In the fibre based distributed plasticity, the RC section contains concrete cover, core and longitudinal bars are divided to small fibres and material properties are assigned to the pre-defined fibres. Unlike distributed plasticity models, in the lumped plasticity models, nonlinear behaviour of RC member is concentrated at the end of them (Banon, et al., 1981; Otani, 1974; Haselton & Center, 2008; Haselton, et al., 2016; Panagiotakos & Fardis, 2001). In this kind of modelling, predefined element nonlinear properties are imposed by a zero-length element as a concentrated plastic hinge. Lumped plasticity models are very efficient to assess seismic behaviour of RC element rapidly and with high accuracy. Several studies have been performed to define appropriate plastic hinge backbone curve parameters for RC columns based on regression of the results of previous experimental studies (Dai, et al., 2020; Kashani, et al., 2016; Berry & Eberhard, 2008).

Co-author of current research have several published researches on the evaluation of corroded RC structures (Roohbakhsh & Kalantari, 2018; Kashani, et al., 2013; Kashani, et al., 2014; Kashani, et al., 2015; Sharma, et al., 2012). Current research has used the results of (Kashani, et al. 2013) during the modelling of the corroded sections. By reviewing the literature, it is evident that a few number of studies have been carried out to develop a lumped plasticity model for corroded RC columns. In one of the recent studies, a new phenomenological lumped plasticity model is developed for corroded rectangular RC columns (Dai, et al., 2020). The model is based on the regression of 103 results of previous experimental studies on rectangular corroded and uncorroded columns. This model can propose lumped plasticity model parameters of corroded columns in comparison with those for uncorroded ones. Compared to previous researches, the developed plastic hinge model for corroded RC columns in this research considering bar modeling details in the corroded section and employing a wide range of design parameters that made the final model more reliable and accurate. Also, developed model is presented for circular column cross section beside rectangular shape which both are common shapes of bridge columns

Accepted Manuscript

1.1 Research novelty and contribution

In the category of distributed plasticity models, the fibre-based models are computationally more efficient and cheaper than continuum FE models. In distributed plasticity modelling, the nonlinearity of material is taken place at each section of element and the overall element behaviour is extracted by using section response at each integration point. (Taucer, et al., 1991) However, for rapid assessment and fragility analysis of a number of bridges or structures after an earthquake, fibre-based models can be very time consuming. Therefore, lumped plasticity models are more efficient for this kind of analysis. Generally, the accuracy of lumped plasticity model which is based on previous experimental results has complete dependency on the number of selected experiments and the range of basic design parameters. Due to lack of important data (i.e., corrosion rate of transvers bars, exact point of section yielding because the lack of longitudinal bars strain recording during the experiment), the accuracy of such of models can be doubtful. Therefore, in this study to overcome the lack of previous studies, a new approach to develop a plastic hinge model for corroded RC columns is presented. In this way, a verified FE procedure is considered to model RC columns from assumed simulation data in parametric study. The simulation data consists of 13440 RC corroded and uncorroded columns with a wide range of design parameters in rectangular and circular cross sections. 1920 of these models are uncorroded and the rest are corroded. Parameters of lumped plasticity model are investigated based on regression of the results of cyclic and monotonic analysis. Finally, the accuracy of calibrated models which are valid for corroded and uncorroded columns are investigated based on the experimental results and numerical models out of the assumed simulation data from parametric study. Results have shown that predicted model can be employed to represent the corroded RC columns nonlinear behaviour with high accuracy.

2. Finite element modelling

An accurate finite element model with distributed plasticity approach is used in this study to model corroded and uncorroded RC columns with circular and rectangular section shapes. The assumed

Accepted Manuscript

procedure for modelling in the level of element and section properties are explained in the following:

Finite element modelling approach proposed by (Kashani, et al., 2016) is used here to model circular and rectangular columns. This model consists of two force-based nonlinear elements with fibre section distributed plasticity scheme. Each element is divided into several sections by implementing integration points.

To decrease the effect of strain localization phenomenon because of post buckling behaviour of steel bars, RC column element is divided into two parts (Figure 2). The length of first part is assumed to be $2L_{eff}$ in rectangular and $6L_{eff}$ in circular cross section columns (Berry & Eberhard, 2008). Based on research by (Coleman & Spacone, 2001) strain localization around plastic hinge region in elements with softening material behaviour such as RC columns may affect the result of column capacity curve completely. To overcome this issue, number and methods of integration points in both elements of RC column are justified. For the first element around the plastic hinge region, two integration points in rectangular cross section column and three integration points in circular cross section column are implemented. For the second element five integration points with Gauss-Lobatto method are considered.

Slippage of longitudinal bars in RC columns play significant role in increasing maximum drift under monotonic or seismic loading and should be considered in the finite element modelling. Based on (Zhao & Sritharan, 2007), a zero-length element is implemented in the base of column model (Figure 2). Complete explanation about modelling and assigning material properties to the zero-length element is available in (Ge, et al., 2020 (a); Ge, et al., 2020 (b)).

Most of the previous studies have just considered the nonlinear behaviour of material in modelling of the corroded RC elements neglecting the important features of inelastic buckling or low cyclic fatigue. The effect of these phenomena can be significant when RC members are corroded. In this study both parameters are contributed in modelling of corroded RC columns.

Accepted Manuscript

2.1 Steel reinforcement model

The general behavior of corroded reinforcement steel material in tension is taken the same as uncorroded material. However, the yield strength or ultimate strain may change accordingly, so the common bilinear behavior of steel material proposed by (Menegotto, 1973; Balan, et al., 1998) is employed for the behavior of material under tension. To consider corrosion effect, yield strength and ultimate strain sustained by longitudinal bars are modified by (Du, et al., 2005 (b)) as follows:

$$\sigma_{y,corr} = (1 - 0.005\psi)\sigma_{y0} \quad (1)$$

$$\varepsilon_{u,corr} = (1 - 0.035\psi)\varepsilon_{u0} \quad (2)$$

Where $\sigma_{y,corr}$ and $\varepsilon_{u,corr}$ represent yield stress and ultimate strain of corroded steel bars respectively. ψ is longitudinal bar mass loss percentage, σ_{y0} and ε_{u0} are yield strength and ultimate strain of uncorroded bars respectively.

To consider the buckling behaviour of longitudinal bars in compression, the model presented by (Dhakal & Maekawa, 2002; Dhakal & Maekawa, 2002) is implemented. In this model the bar buckling behaviour in compression is justified by λ_p coefficient:

$$\lambda_p = \sqrt{\frac{\sigma_y}{100}}\left(\frac{L_{eff}}{D}\right) \quad (3)$$

Where σ_y is yield strength of steel bars, D is bar diameter and L_{eff} is longitudinal bars effective buckling length. The effect of corrosion on the buckling behaviour of corroded steel bars under compression has been investigated by (Kashani, et al., 2014). In this method λ_p is modified by the following equations:

Accepted Manuscript

$$\lambda_{p,corr} = \sqrt{\frac{\sigma_{y,corr}}{100}}\left(\frac{L_{eff}}{D_{corr}}\right) \quad (4)$$

$$D_{corr} = D_0(1-0.01\psi) \quad (5)$$

$$\sigma_{y,corr} = \begin{cases} \sigma_y(1-0.005\psi) & \frac{L_{eff}}{D_{corr}} \le 5 \\ \sigma_y(1-0.0065\psi) & 5 < \frac{L_{eff}}{D_{corr}} \le 10 \\ \sigma_y(1-0.0125\psi) & 10 < \frac{L_{eff}}{D_{corr}} \end{cases} \quad (6)$$

Where ψ is longitudinal bars mass loss percentage and D_0 is diameter of uncorroded bar. As mentioned previously, L_{eff} is the effective buckling length of steel bars. It depends on different parameters such as diameter, stiffness and spacing of transvers bars. have conducted a research to investigate L_{eff} as a coefficient of transvers bars spacing. This method is used here to find L_{eff} .

For modelling cyclic response of steel bars, *Hysteretic material* in Opensees (McKenna, 2011) platform is implemented. Pinching effect in the cyclic stress-strain behaviour of steel reinforcement play a significant role in generic degradation of RC members under cyclic loads. There are two key pinching parameters to consider cyclic behaviour in *Hysteretic material.* The pinching parameters for corroded steel bars and the calibrated values by (Kashani, et al., 2014), are used in this study. Further explanation about pinching behaviour of steel reinforcement is available in (Kashani, et al., 2015). Strength loss due to Low-cyclic fatigue is another important phenomenon that should be considered in modelling of corroded steel bars. for this purpose, here,

Accepted Manuscript

uniaxial fatigue material is employed in Opensees (McKenna, 2011). Parameters in fatigue material are modified to consider corrosion effect based on (Kashani, et al., 2015).

2.2 Concrete material model

Concrete02 material model is implemented to model the unconfined concrete. By initiation of corrosion in steel bar, rust material as a result of corrosion accumulates around the steel bar.

This phenomenon imposes extra tension stresses on the concrete in the surrounding of the steel bars and leads to cover cracks and spalling (Guo, 2011). Thus, it is necessary to consider corrosion effects on the concrete cover. (Coronelli & Gambarova, 2004) proposed the following equation to modify concrete cover compressive strength affected by corrosion.

$$\sigma_c^{'} = \frac{\sigma_c}{1 + k\frac{\varepsilon_1}{\varepsilon_0}} \quad (7)$$

Where $\sigma_c^{'}$ and σ_c are compressive strength of corroded and uncorroded concrete cover respectively, k is a coefficient that depends on the type of bars and is suggested to be equal to 0.1, ε_0 is concrete cover strain corresponding to σ_c and ε_1 is calculated by the following equations.

$$\varepsilon_1 = \frac{P_{corr} - P_0}{P_0} \quad (8)$$

$$P_{corr} - P_0 = N_{bars} W_{cr} \quad (9)$$

$$W_{cr} = 2\pi(\upsilon_{rust} - 1)X \quad (10)$$

Accepted Manuscript

Where P_{corr} and P_0 are corroded and uncorroded section perimeter respectively, N_{bars} is number of bars in the section, W_{cr} is crack width in the depth of X and υ_{rust} is portion of corroded bar value to uncorroded value.

Transvers bars produce appropriate confining for concrete core in the RC section. (Scott, 1982) presented following equation to increase the compressive strength of confined concrete with *k* coefficient:

$$k = 1 + \frac{\rho_s f_{yh}}{f_c^{'}} \quad (11)$$

Where f_{yh} is yield strength of transvers bars, ρ_s is volumetric ratio of transvers bars. In this study to consider corrosion effect on the confined concrete, a simple method is implemented. Based on this method, the volumetric ratio and yield strength of transvers bars are modified based on the following equations:

$$f_{yh,corr} = (1 - 0.005\psi_h) f_{yh0} \quad (12)$$

$$D_t = D_{t0}(1 - 0.01\psi_h) \quad (13)$$

Where $f_{yh,corr}$ and f_{yh0} are yield strength of corroded and uncorroded transvers bars respectively, D_t and D_{t0} are diameter of corroded and uncorroded transvers bars respectively and ψ_h is mass loss percentage of transvers bars.

3. Verification of fibre-based finite element model

To implement the mentioned FE model for further assessing, it is necessary to validate the model with experimental studies. Experimental studies by (Mo & Wang, 2000) (column C1-1) and (Meda,

Accepted Manuscript

et al., 2014) (corroded and uncorroded columns) are selected to control the mentioned FE model for rectangular RC columns. Details of the mentioned experimental studies are summarized in Table 1. Mo et al. used 400*400 mm^2 section with the length to depth ratio of 3.5. 300*300 mm^2 sections were studied by (Meda, et al., 2014) with a value of 6 for length to depth ratio. As for the circular RC columns model, experimental studies by (Moyer & Kowalsky, 2003). (No. 1 column) and (Lehman, 2000) (column 415) are selected. They employed 457.2 mm section diameter with a length to depth ratio of 5.33 and 609.6 mm section diameter with a length to depth ratio of 4 respectively. Details for these elements also are summarized in Table 1. The results of comparison between proposed model and experimental results are illustrated in Figure 3 for rectangular and circular columns.

As observed, the results of cyclic behaviour of RC columns when modelled using the proposed fibre-based FE procedure, are close enough to those of experimental results. This consistency between results of two cases shows the capability of the FE model to be used for further assessing in the following.

4. Column models of parametric study

As mentioned previously, to have a reliable lumped plasticity model of RC columns under corrosion, it is important to consider appropriate specimens in the simulation data from parametric study. To achieve this, several design parameters are considered to vary in all models in the simulation data. Parameters include axial load ratio, concrete compressive strength, yield and ultimate strength of longitudinal and transvers bars, longitudinal bar ratio, section effective depth and volumetric ratio of transvers bars. Damage rate because of corrosion is considered as mass loss ratio of longitudinal bars. To assess the impact of each mentioned parameter on the final model, it is necessary to assume a credible and comprehensive range of each parameter.

Detailed properties of such RC columns as RC bridge piers are presented in Table 2 and employed in the parametric study. Figure 2 demonstrates schematic view and section of RC columns with circular and rectangular cross sections. This shape could be related to a bridge pier which is presented in Figure 1.

Accepted Manuscript

4.1 Axial load ratio

Minimum value that has been considered for axial load is $0.05A_g f_c^{'}$, where A_g is section gross area and $f_c^{'}$ is concrete compressive strength. Based on (ACI committee & International Organization for Standardization, , 2019), axial load of $0.3A_g f_c^{'}$ can be approximately corresponded to the beginning of compression control behaviour. Therefore, in current study to consider bending-compression behaviour, the maximum value of $0.3A_g f_c^{'}$ is used for axial load.

4.2 Longitudinal bar ratio

As mentioned in ACI-318, longitudinal bar ratio in beam-column elements has a value between 0.005 A_g to 0.08 A_g. To consider splicing, the maximum value is limited to 0.04 A_g. In current study to observe ACI limitation, a range between 0.01 to 0.03 of column gross section area is selected for longitudinal bar ratio.

4.3 Longitudinal and transvers bar strength

Three grade of steel bars including S340, S400 and S500 are used for longitudinal steel bars in the models with ultimate strength of 500, 600 and 650 MPa respectively. For transvers bars, two types of S340 and S400 grades are considered.

4.4 Concrete compressive strength

Based on (ACI committee & International Organization for Standardization, , 2019), minimum value of concrete compressive strength can be 2500 psi or 17 MPa. In current study a range of 20 to 50 MPa is assumed for concrete compression strength.

4.5 Volumetric ratio of transvers bars

Range between 0.0015 through 0.009 is considered for volumetric ratio of transvers bars in this study which represent sections from low-confined through well-confined RC column configurations.

4.6 Corrosion damage

Accepted Manuscript

In the current research, the damage of corrosion is presented as mass loss percentage of longitudinal steel bars. $\psi(t)$ is calculated based on the following equation:

$$\psi(t) = (1 - (\frac{D(t)}{D_0})^2) \times 100 \quad (14)$$

Where $D(t)$ is bar diameter after corrosion and D_0 is intact bar diameter. $D(t)$ can be calculated by direct measurement of corroded bar diameter or based on the analytical equation which represents $D(t)$ based on the corrosion rate. Corrosion rate also dependents on several parameters such as water to cement ratio and concrete cover thickness. More related information in this regard are presented in (Vu & Stewart, 2000). To consider different levels of corrosion damage, steel bar mass loss percentage varies between 0 to 24 percent. More details of the mentioned design parameters considered for circular and rectangular sections are available in (Table 2).

4.7 Effect of cross section dimension

To consider the effect of cross section dimension on the lamped plasticity model, several sections with different dimensions consist of circular and rectangular shapes are defined in the simulation data from parametric study. In this way, sections width with a range between 250mm through 1500mm are considered for circular and rectangular columns. Final lumped plasticity model revealed that effective depth (*d*) of column section has significant impact on the force-based parameters (i.e. moment) of plastic hinge model. Further information about consideration of section dimension and fitting procedure are presented in section 8.

5. Properties of the selected hysteretic deterioration model

There are several verified hysteretic lumped plasticity models in the literature (Wang, et al., 2001; Song & Pincheira, 2000; Kunnath, et al., 1990; Ramberg & Osgood, 1943). Among them, a few consider important phenomena such as strength and stiffness deterioration comprehensively. (Ibarra, et al., 2005) presented a simple hysteretic model that consider stiffness and strength

Accepted Manuscript

deterioration properly under cyclic loads such as earthquake. Ibarra's hysteretic model is developed for systems with different behaviour such as peak-oriented, bilinear and pinching. This model has been utilized by other researchers in the last years. Figure 4 illustrates Ibarra's model which can be summarized in two major parts: a) a trilinear backbone model that shows basic key points of strength and deformation of the system and, b) several equations that present hysteretic deterioration between key points. Recently several researchers tried to present a refinement to the Ibarra's original model. (Lignos, 2008) presented a modification on the original model that is named as modified Ibarra Krawinkler model. modifications that have been considered in the modified Ibarra Krawinkler model can be summarized in the following steps:

1) in the backbone curve, the value of ductility ratio $\left(\delta_c / \delta_y\right)$ is changed by deformation of the system in the strength capacity δ_p, 2) in the backbone curve, instead of strain hardening coefficient in the original model, a ratio of minimum strength capacity to yield strength $\left(F_c / F_y\right)$ is used.,3) in the backbone curve, post capping coefficient (α_c) in the original model is changed by post capping deformation (δ_{pc}), 4) original Ibarra's model in cyclic deterioration phase is refined to be capable for systems with asymmetric behaviour in negative and positive branch, and 5) definition of energy dissipation capacity in modified Ibarra Krawinkler model (E_t) is changed to be based on δ_p rather than δ_y.

(Lignos, 2008) calibrated his model for 200 RC components based on peak-oriented method and presented *ModlMKPeakOriented* material in the Opensees platform (McKenna, 2011) as a result. In the current study, modified Ibarra-Krawinkler model with peak oriented method is employed to present hysteretic model of corroded RC columns. Based on the illustration of (Figure 5) 23 key parameters are required to produce lumped plasticity model. These parameters can be classified in two major categories of monotonic parameters and cyclic deterioration parameters. Detailed description of parameters is available in (Tables 3 and 4)

Accepted Manuscript

6. Procedure to calibrate the model

6.1 Monotonic parameters

As mentioned previously, modified Ibarra-Krawinkler model (Lignos, 2008) with peak-oriented method is selected to produce calibrated lumped plasticity model of corroded RC columns. Modified Ibarra-Krawinkler (Lignos, 2008) model is a monotonic trilinear backbone curve with consideration of cyclic deterioration in the system. As recommended by researchers (Lignos, 2008) and (Dai, et al., 2020), it's appropriate to calibrate modified Ibarra-Krawinkler model for a system by contributing results of both cyclic and monotonic analysis. In the previous research on the calibration of RC model which are based on experimental analysis results (Haselton, et al., 2016) and (Dai, et al., 2020), because of lack of monotonic experimental analysis results, monotonic parameters have been defined based on cyclic results by self-judgment.

Figure 6 illustrates results of monotonic and cyclic analysis of the No. 411 rectangular column from assumed simulation data. This column is without corrosion and its details are summarized in Table 5. The figure at first glance shows significant differences between cyclic and monotonic curves in deterioration part. The figure proves the effect of cyclic deterioration which is not accessible with monotonic analysis result alone. Hence, cyclic deterioration and monotonic results must be contributed to calibrate the final model. based on procedure presented by (Haselton, et al., 2008), the five important parameters including yield moment and rotation (M_y and θ_y), hardening stiffness (K_s), capping rotation (θ_{cap}), and post capping stiffness (K_c) should be calibrated by contributing monotonic analysis result.

The yield point of RC column model is a point on the monotonic or cyclic curve behaviour which corresponds to the yielding of steel bars in tension or when concrete strain reaches to 0.002 (Applied Technology Council, 2017). By defining the yield moment and rotation, elastic stiffness (K_0) could be resulted. As illustrated on Figure 6, the yield point (point No. 1) is approximately at the location where the slope of tangent line changes significantly. This method has been introduced by (Haselton, et al., 2008) for calibration models based on experimental cyclic results without any information about yielding point of longitudinal bars.

Accepted Manuscript

Capping point is a point in the cyclic behaviour curve which is followed by negative tangent slope (point No. 2 in Figure 6). In other words, the capping point is followed by significant strength deterioration in the system cyclic curve which is called in-cycle deterioration (Haselton, et al., 2008).

Hardening stiffness is an important parameter which is used to define plastic hinge model behaviour after yield point. As mentioned previously, the final plastic hinge model can be used to assess the RC structure rapidly with high accuracy. Hardening stiffness is usually defined as a portion of elastic stiffness. In current study the actual value of hardening stiffness is taken as the slope of connecting line between yield point and capping point.

(Haselton, et al., 2016) have suggested that negative stiffness of post capping line could be defined by visual fitting a tangent line based on the observed significant cyclic deterioration. (Fardis & Biskinis, 2003) and (Panagiotakos & Fardis, 2001) recommended that post-capping point is a location in which %20 strength loss occurs from capping in the monotonic or cyclic analysis results and expressing that the post-capping stiffness could be defined based on the coordinate of the post-capping and capping point. In current study post-capping stiffness is defined based on negative tangent slope after capping point and a location in which %20 strength loss (point No. 3 in Figure 6) is occurred.

6.1 Cyclic parameters

Cyclic deterioration parameters including λ and C (four different values for each parameter which are mentioned in Table 3) could be calibrated by visual fitting of observed deterioration in cyclic analysis result. (Haselton, 2006) emphasized that for RC columns failing in flexure a value of 1.0 and for columns failing in flexure and shear a value of 1.2 is ideal for all C_s, C_c, C_A and C_k parameters. For consistency a value of C=1.0 is considered for all columns in the current study. This assumption has also been considered by (Haselton, 2006). λ_s, λ_c, λ_A and λ_k are other important parameters to simulate cyclic deterioration. Based on previous research suggestions and (Lignos & Krawinkler, 2011) and (Dai, et al., 2020), these four parameters could be considered as constant value of λ. To calibrate λ value for each model in the simulation data from parametric study, the following procedure is implemented:

Accepted Manuscript

a) the RC column is modelled by imposing concentrated plastic hinge data (monotonic data that have been defined previously)

b) Cyclic deterioration parameter (λ), has been considered as a value of 0.05 in the modelling

c) Cyclic analysis is performed using the model and moment-rotation result is extracted.

d) The cyclic moment-rotation analysis result of concentrated plasticity modelling is compared with moment-rotation results of the model with a distributed plasticity. If the results in deterioration part match each other, the appropriate (λ) is reported. Otherwise (λ) value is increased 0.25 and the procedure is repeated from step (b). (note: (Lignos, 2008) reported that (λ) value for RC beam-column elements usually has a value between 0 and 4)

Figure 7 illustrates a procedure to find appropriate (λ) value for the No. 411 rectangular RC column. This column is without corrosion and its details are summarized in Table 5. Generally, the mentioned procedure for calibrating cyclic deterioration parameter in uncorroded column sample is the same as corroded one. For briefing the values of (λ) lower than 2 are eliminated in Figure 7. It is evident that, in this model by increasing (λ) value, deterioration part of cyclic curve could be calibrated better with the main model and the value of 3.75 is the best choice for matching with reference model.

7. Calibration results

After identification and calibration of parameters that are necessary to define the lumped plasticity model, it is important to know about the effect of first design parameters on hysteretic behaviour of corroded RC columns. This may guide the researcher to find a better final empirical model that reflects the effect of design parameters properly. Therefore, in this way the relation of key parameters such as yield moment and rotation (M_y and θ_y), capping moment and rotation (M_p and θ_p) and post-capping rotation (θ_{pc}) to the design parameters are assessed. To summarize, just the relation of axial load ratio, longitudinal bar ratio and concrete compressive strength to the mentioned parameters are presented here. The results are presented in Figures 7 through 9. In these illustrations, calibration results are presented as height of bar charts. As the goal of current

Accepted Manuscript

study is to develop an appropriate lumped plasticity model for corroded RC columns, corrosion damage is mentioned on each Figure to illustrate simultaneous effect. As discussed previously, 13440 circular and rectangular RC columns are modelled in the current study. Because of large number of models, each bar chart in the following figures is representative of average of results for a special category. (i.e., in Figure 8 (a), there are 7 categories of corrosion damage and 4 categories of axial load ratio that ensemble 28 categories in total. This means each bar chart value in this Figure is an average of 480 sample results). In Figure 8, the simultaneous effect of corrosion damage and axial load ratio on the calibrated parameters are presented. As it is clear, by increasing corrosion, all calibrated value of moment and rotation decrease significantly. This Figure also indicates that increasing axial load ratio may reduce values of capping and post-capping rotation.

Figure 9 illustrates the effect of longitudinal bar ratio on the calibrated parameters. Based on the Figure, low reinforced RC columns, have a lower value of yield and capping moment and yield rotation than highly reinforced columns. It also could be extracted from Figure 9 that the effect of longitudinal bar rotation on the capping and post-capping rotation is less tangible when RC column is highly corroded.

Concrete compressive strength is another important design parameter which was investigated in this study. As illustrated in Figure 10, RC columns with larger concrete compressive strength have lower value of yield, capping and post-capping rotation. It should be noted that in highly corroded elements this reduction is more intangible.

8. Regression procedure and results

8.1 Monotonic behaviour parameters

In the current study a regression procedure has been conducted to develop appropriate empirical relations for parameters of lumped plasticity model in corroded RC columns. This regression procedure has been performed on the calibrated parameters to find the best prediction based on the design parameters. The final empirical prediction will be capable to produce lumped plasticity model. As mentioned in the previous parts, design parameters such as axial load ratio (ν),

Accepted Manuscript

longitudinal bar ratio (ρ_v), longitudinal bar yield and ultimate strength (f_y and f_u), concrete compressive strength ($f_c^{'}$), transvers bars yield and ultimate strength (f_{yh} and f_{uh}), transverse bars volumetric ratio (ρ_h), section effective depth (d) and corrosion damage level (mass loss ratio of longitudinal bar) are considered as the main variables. To find empirical relation to express lumped plasticity model of corroded RC columns, it is necessary to define the best prediction for lumped plasticity parameters such as yield moment and rotation (M_y and θ_y), capping moment and rotation (M_p and θ_p) and post-capping rotation (θ_{pc}). Cyclic deterioration parameter is also required to be estimated to find deterioration segment behaviour.

A multivariable equation is considered as objective function to find empirical prediction. This function is assumed as linear form with or without interaction between variables. These two types of equations can be presented as:

$$y = \alpha_0 + \alpha_1 x_1 + ... + \alpha_n x_n + \varepsilon \quad (15)$$

$$y = \alpha_0 + \alpha_1 x_1 x_2 + ... + \alpha_n x_m x_n + \varepsilon \quad (16)$$

Where (y) is the prediction of calibrated parameter, x_1 to x_n are design parameters and ε is random error. To find the most accurate value of $\alpha_{(0 \text{ through n})}$ coefficients in the above functions, a try and error procedure is conducted. Stepwise regression method with linear initial terms and interaction upper bond terms is implemented for regression procedure. In the stepwise method, unnecessary parameters in prediction are trimmed automatically (Chatterjee & Hadi, 2015). The elimination is based on p-value parameter as each quantity with higher p-value are less important ones and trimmed.

As discussed in section 4 previously, cross section dimension is a design parameter that has been considered in simulation data from parametric study. This parameter has significant impact on the force-based parameters of plastic hinge model which are obvious in the above empirical equations. Figures 11 and 12 show dependency between force-based (moment) quantity of

Accepted Manuscript

plastic hinge model for rectangular and circular cross sections respectively. As it is obvious, the yield and capping moment have a parabolic dependency with effective depth of column. By fitting a parabolic function, a coefficient is resulted for moment quantity of plastic hinge model. these coefficient functions are presented in the following:

Rectangular cross section: $M_y \,\&\, M_p \propto (15.9d^2 - 6.7d + 1)$

(17)

Circular cross section: $M_y \,\&\, M_p \propto (5.2d^2 - 2.5d + 0.5)$

(18)

In this study, two types of cross section shape are considered and the final empirical equations are presented for circular and rectangular cross section shapes as following:

Circular columns:

$$\theta_y = 0.0042 - \frac{\psi}{21130} + \frac{\upsilon}{168.4} + \rho_v\left(\frac{f_y}{1491} - 0.17\right) + \frac{1}{20.3 f_c} - \frac{\rho_h f_{yh}}{36181}$$

(19)

$$M_y = (5.2d^2 - 2.5d + 0.5)(-47.8 - 12.9\psi + 1510.7\upsilon + 52.7\rho_v f_y + 12.3 f_c)$$

(20)

$$\theta_p = \coth(0.15(\psi + 10))\left\{-0.069 + 0.005\rho_v f_y + \frac{0.175}{\upsilon f_c} + 0.053\rho_h f_{yh}\right\} + \rho_v f_y\left\{-0.005 - \frac{0.0004}{\upsilon f_c} - \frac{\rho_h f_{yh}}{47047}\right\} + \rho_h f_{yh}\left(\frac{0.002}{\upsilon f_c} - 0.053\right) - \frac{0.169}{\upsilon f_c} + 0.074$$

(21)

$$M_p = (5.2d^2 - 2.5d + 0.5)(-33.7 - 10\psi + 1239\upsilon + 58.9\rho_v f_y + 11.9 f_c)$$

(22)

Accepted Manuscript

456 $$\theta_{pc} = \coth(0.15(\psi + 10))\left\{-0.084 + 0.008\rho_v f_y + \frac{0.282}{\upsilon f_c} + 0.064\rho_h f_{yh}\right\} + \frac{1}{\upsilon f_c}\left\{-0.274 + \frac{\rho_v f_y}{6959} + 0.002\rho_h f_{yh}\right\} - 0.007\rho_v f_y - 0.064\rho_h f_{yh} + 0.090$$

457 (23)

458 Rectangular columns:

459 $$\theta_y = 0.0022 - \frac{\psi}{11516} + \frac{\upsilon}{141.3} + \rho_v\left(\frac{f_y}{1246} - 0.18\right) + \frac{1}{12.3 f_c} - \frac{\rho_h f_{yh}}{14257}$$

460 (24)

461 $$M_y = (15.9d^2 - 6.7d + 1)(-12.5 - 7.4\psi + 886.2\upsilon + 23.6\rho_v f_y + 6.8 f_c)$$

462 (25)

463 $$\theta_p = \coth(0.05\psi + 1)\left\{1.16 - 2.61\rho_v + 0.21\frac{f_c}{f_y} - 1.18\upsilon^{0.05}\right\} + \rho_v\left\{-5.93 - 2.11\frac{f_c}{f_y} + 9.69\upsilon^{0.05}\right\} + \frac{f_c}{f_y}\left\{1.47 - 1.82\upsilon^{0.05}\right\} + 1.02\upsilon^{0.05} - 1$$

464 (26)

465 $$M_p = (15.9d^2 - 6.7d + 1)(31.1 - 9.7\psi + 711.4\upsilon + 28.3\rho_v f_y + 6.5 f_c)$$

466 (27)

467 $$\theta_{pc} = \psi^2\left\{\frac{\upsilon^{0.05}}{949} + \frac{\rho_v f_y}{302070} - \frac{\rho_h}{827590} - \frac{1}{987}\right\} + \upsilon^{0.05}\left\{0.03\rho_v f_y - 8.1\rho_h - 0.96\right\} - 0.03\rho_v f_y\left\{\rho_h + 1\right\} + 8.25\rho_h + 0.92$$

468 (28)

469 As it is clear in the predicted equations for capping and post-capping rotation in circular columns
470 and also capping rotation of rectangular columns, there is a term of hyperbolic cotangent of
471 corrosion damage parameter. This selection is because of special dependency of the mentioned
472 calibrated parameters on the corrosion damage level. As an example, capping rotation is plotted
473 for all circular columns in Figure 13 and corrosion level of columns are separated by different

Accepted Manuscript

colours. As it observed, by increasing corrosion level, capping rotation decreases with very close behaviour to the tangent function.

To assess the accuracy of predicted empirical equations, the calculated values by the derived equations are compared with the responses obtained from calibration. The results of compression are illustrated in Figures 14 and 15 for rectangular and circular columns respectively. θ_y, M_y, θ_p, M_p and θ_{pc} are predicted parameters which are presented in the mentioned Figures. Statistical parameters such as mean (μ), median, standard deviation (σ) and R-squared factor (R^2) also could present the accuracy of the predicted functions. In this way the ratio of calibrated to predicted responses are calculated and their associated statistical responses are summarized in the Table 6

8.2 Cyclic deterioration parameters

As described in the previous sections, to consider cyclic deterioration in lumped plasticity model, (λ) parameter is calibrated based on cyclic analysis results. Linear regression procedure with stepwise scheme is also implemented on the calibrated results of (λ) parameter and an empirical equation are presented with acceptable accuracy for this parameter. The empirical functions are reported for circular and rectangular cross sections separately in following functions.

$$\lambda_{rec} = 0.28 + 0.12\coth(\psi + 0.1) + 0.004\frac{f_c}{\upsilon} - 20.8\rho_v + 49.86\rho_h \quad (29)$$

$$\lambda_{cir} = -0.188 + \psi(0.132 - 0.028\rho_v f_y) + 0.293\rho_v f_y + 0.265\rho_h f_{yh} \quad (30)$$

As it is obvious, cyclic deterioration parameter in RC columns with rectangular section is depended on corrosion intensity, concrete compressive strength, axial load ratio and longitudinal and transvers bar ratio. While in circular columns it depends on corrosion damage ratio, longitudinal and transvers bars ratio and yield strength. The R-squared factor for rectangular and circular columns for above empirical equations are obtained 53 and 45 respectively.

Accepted Manuscript

9. Verifying the accuracy of empirical model

To verify the developed empirical models, it is necessary to evaluate the cyclic behaviour by simulating models that have not been in the assumed simulation data from parametric study. In this way, several RC rectangular and circular columns with and without corrosion effects are simulated using empirical equations. These columns could be classified in two main parts, numerical models which are out of assumed simulation data for model calibration and previous experimental models which are available in the literature. This procedure is discussed in two parts in the following:

9.1 Verification with the numerical models out of assumed simulation data

6 rectangular and 5 circular columns are considered for validation in this part. Details of these columns are somehow selected which are not similar to assumed columns in the simulation data from parametric study. Columns details are collected in the Table 7. They are modelled using empirical equations to define lumped plasticity parameters of a concentrated plastic hinge. Modified Ibarra-Krawinkler model with peak oriented method (Lignos, 2008) is used in Opensees (McKenna, 2011) platform for modelling the plastic hinge behaviour. Symmetric cyclic loading protocol of (ACI Committee, 2005) demonstrated in Figure 16 is implemented here. Figures 17 and 18 show hysteretic behaviour resulted from current proposed model and the fibre based element with distributed plasticity.

As it is obvious in Figures 16 and 17, the results of hysteretic behaviour of RC columns simulated using the proposed models are close to those responses of the fibre-based elements with distributed plasticity. This shows the accuracy of empirical model to simulate cyclic behaviour of RC corroded and uncorroded columns.

9.2 Validation with experimental studies

To validate the proposed plastic hinge model for corroded and uncorroded RC columns model, previous experimental studies available in the literature that have been presented in third section, are used here. Details for these elements also are summarized in Table 1. The results of

Accepted Manuscript

comparison between proposed plastic hinge model and experimental results are illustrated in Figure 19 for rectangular and circular columns.

As observed, the results of cyclic behaviour of RC columns when modelled using the proposed equations are close enough to those of experimental results. This consistency between results of the two cases shows the capability of the new model to simulate the corroded and uncorroded elements with an acceptable accuracy.

9.3 Validation with a bridge experimental model

To examine the developed plastic hinge model in a real RC structure, the hinge model is implemented in Johnson's bridge experimental study (Johnson, 2006). This bridge is designed by utilizing NCHRP (12-49) (Mayes & Friedland, 2002) and model with a quarter scale that made it capable for shake table test. The bridge prototype consists of two spans and three piers. Each pier consists of two circular columns. Piers have different heights that making the whole bridge asymmetric. Bridge girders are post-tensioned RC box and connections between cap-beams and deck are in monolithic form. Bridge model has no abutments in sideways. Total length of bridge is 20.5m and each span has 9.14m length. Clear lengths of columns are 2.44m, 1.83m and 1.52m for middle and sides bents respectively. Bridge deck consists of three box RC girder with 0.76m width and 0.38m depth. Longitudinal and transvers bar ratio of columns are 1.56 and 0.9 percent respectively. Total length and depth of cap-beams are 2.49m and 0.38m respectively. Superstructure of the bridge is loaded by different blocks with weights of 107kN, 87kN and 22.7kN. Compressive strength of confined concrete used in this bridge is 40.7MPa. Average value of yield and ultimate strength of all reinforcement are 462MPa and 552MPa respectively. More details of bridge description and so section dimension are presented in Figure 20.

A 3D model of mentioned bridge is implemented in Opensees platform. This model is such that all nonlinearities of bridge behaviour are concentrated in columns. This assumption is not incoherent with this fact that deck and cap-beams are stiff enough in comparison with columns. Nonlinearity of columns are concentrated in plastic hinges at their connection region to footing and cap-beams. Plastic hinge properties are extracted from the developed model in this study based on columns design parameters which are summarized in Table 8. Superimposed loads are

Accepted Manuscript

554 assigned to ten nodes above the deck exactly in the centre of mass of blocks. These nodes are
555 connected by rigid link to the bridge deck. FE model configuration are presented in Figure 20 (b).
556 Northridge 1994 earthquake motion (shortened and modified based on soil type) has been
557 selected in Johnson's study. As emphasized by (Zadeh & Saiidi, 2007), because of interaction
558 between bridge piers and shake table, the recorded shake table motion during the test was
559 incoherent with input motion. So it is recommended to use shake table recorded displacement
560 during the test as input excitation in Opensees. (Zadeh & Saiidi, 2007) declared that displacement
561 input in time history analysis, results high inherent damping in the structures. So in current study
562 damping ratio of %2 is used in finite element modelling. Figure 21 presents measured
563 displacement of three shake tables during test #16 which are used in current study as input
564 excitation. (Johnson, 2006) implemented several shake table tests on the mentioned experimental
565 bridge. Tests are divided in two parts, low amplitudes and high amplitudes. In high amplitudes
566 part, eleven motions are imposed to the model in two days (test #12 through #22). In current study
567 to consider residual damages because of previous tests, all motions of high amplitude part are
568 imposed to the FE model and a rest time of 25s is considered between them. As reported by
569 (Johnson, 2006) residual damages during low amplitude motions are infinitesimal, they are
570 neglected in FE modelling in current study.

571 Static analysis and dynamic time history analysis of FE bridge model are compared with
572 experimental results. (Johnson, 2006) reported first four time periods and corresponding
573 frequencies of the bridge experimental model by utilizing free vibration testing. These values are
574 compared with achieved values of FE model in current study (Table 9). As it is obvious the
575 calculated time periods of FE model are close enough to the results of experimental study. To
576 examine the dynamic behaviour of FE bridge model, shake table test #16 is selected from
577 (Johnson, 2006). in this one directional shake table test, all piers are accelerated in transvers
578 direction. As mentioned previously, shake tables displacement are used as input motion in FE
579 model. by employing time history analysis on the FE model of bridge, drift of all piers are recorded.
580 These results are compared with experimental results by (Johnson, 2006) in Figures 21 through
581 23.

Accepted Manuscript

As it is obvious, based on results presented in Figure 22 through 24, calculated dynamic time history analysis are close enough to experimental results. i.e. in the test #16 maximum calculated absolute value of drift for bent 3 (which is the shortest pier) is 0.026 and this value is 0.03 for experimental study. For middle bent (the highest pier) these values are 0.025 and 0.04 for experimental and current study calculated results respectively.

10. Summary and conclusion

An empirical plastic hinge model for corroded RC columns is developed in this study. The model requires section property, material property and corrosion mass loss data to propose the characteristic of the plastic hinge during hysteretic excitation. The procedure of development of the model is summarized in the following steps:

a) 13440 RC column models with circular and rectangular cross sections are considered in the simulation data from parametric study. These numerical samples with a wide range of design parameters such as axial load ratio, rebars properties, concrete properties and a wide range of corrosion from uncorroded to %24 mass loss of longitudinal bars.

b) finite element model has been implemented with distributed plasticity scheme for each sample by taking into account the important degradation characteristic such as buckling of longitudinal bars and low cyclic fatigue.

c) key parameters of trilinear lumped plasticity model such as yield moment and rotation, capping moment and rotation and also cyclic deterioration parameter are calibrated by using the hysteretic and monotonic analyses results.

d) stepwise regression method with linear initial terms and interaction upper bonds terms is conducted to find an appropriate empirical prediction of lumped plasticity calibrated parameters. Finally, the empirical equations are presented as a function of RC columns design parameters and corrosion damage rate.

e) the accuracy of empirical model is validated by using numerical models which are not in the simulation data and also experimental models which are available in the literature. Also an

Accepted Manuscript

experimental bridge model is selected for validation of empirical developed model. Comparison between results of empirical model and model in validation procedure has shown very close consistency.

According to the result of this study, final conclusion could be presented in the following steps:

- Aging RC columns which are exposed to chloride-induced corrosion are more vulnerable in the cyclic loading such as earthquake. The predicted empirical equation which is presented in this study, could evaluate the effect of corrosion on the hysteretic behaviour of corroded RC columns with high efficiency.
- The analytical results of cyclic and monotonic analyses in this study proved that corrosion can affect key parameters of lumped plasticity model significantly. i.e., corrosion reduces capping and post-capping rotation. This reduction is more tangible in the higher level of axial load ratio. Such as mentioned examples, the effect of corrosion on the parameters of lumped plasticity model are evaluated by considering all important design parameters.
- numerical modeling approaches which are based on the concentrated plastic hinge can predict structural behavior requiring less analysis cost with acceptable accuracy. So this method is highly regarded by engineers. Most of RC bridges in areas prone to corrosion suffer severe damage in piers and other parts. After estimating the corrosion damage level in the corroded columns, the newly developed plastic hinge model may be employed to model and assess the bridge corroded columns performance with an acceptable accuracy and analysis cost. The result of such method can be appropriate for further assessment studies such as fragility analysis.

Acknowledgements

The research described in this paper was partially supported by the Iran National Science Foundation under the Grant No. 98002792. As RC structures in many areas of Iran are prone to corrosion due to chloride ion attack. This grant has been approved to gain the required knowledge and develop a simplified approach to modeling and assessment of such structures. In this regard the objective of current study has been focused on development of lumped plasticity modeling technique with acceptable efficiency and accuracy.

Accepted Manuscript

References

ACI committee & International Organization for Standardization, , 2019. *Building code requirements for structural concrete (ACI 318-08) and commentary.*

ACI Committee, 2005. *Acceptance Criteria for moment frames based on structutral testing and commentary. ACI, 374, 1-05.*

Afsar Dizaj, E., Madandoust, R. & Kashani, M. M., 2018. Exploring the impact of chloride-induced corrosion on seismic damage limit states and residual capacity of reinforced concrete structures. *Structure and Infrastructure Engineering,* Volume 14, p. 714–729.

Alipour, A., Shafei, B. & Shinozuka, M., 2011. Performance evaluation of deteriorating highway bridges located in high seismic areas. *Journal of Bridge Engineering,* Volume 16, p. 597–611.

Applied Technology Council, 2017. *guidelines for nonlinear structural analysis for design of buildings, part IIb- reinforced concrete moment frames (NIST GCR 17-917-46v3).* s.l.:National Institute of Standard and Technology (NIST).

Balan, T. A., Filippou, F. C. & Popov, E. P., 1998. Hysteretic model of ordinary and high-strength reinforcing steel. *Journal of Structural Engineering,* Volume 124, p. 288–297.

Banon, H., Biggs, J. M. & Irvine, H. M., 1981. Seismic damage in reinforced concrete frames. *Journal of the Structural Division,* Volume 107, p. 1713–1729.

Berry, M. P. & Eberhard, M. O., 2008. Performance Modeling Strategies for Modern Reinforced Concrete Bridge. *University of California, Berkeley.*

Cardone, D., Perrone, G. & Sofia, S., 2013. Experimental and numerical studies on the cyclic behavior of R/C hollow bridge piers with corroded rebars. *Earthquakes and Structures,* Volume 4, p. 41–62.

Accepted Manuscript

662 Chang, Z. Q., Xing, G. H., Luo, D. M. & Liu, B. Q., 2020. Seismic behaviour and strength
663 prediction of corroded RC columns subjected to cyclic loading. *Magazine of Concrete*
664 *Research,* Volume 72, p. 900–918.

665 Chatterjee, S. & Hadi, A. S., 2015. *Regression analysis by example.* John Wiley & Sons.

666 Clough, R. W. & Benuska, K. L., 1967. Nonlinear earthquake behavior of tall buildings.
667 *Journal of the Engineering Mechanics Division,* Volume 93, p. 129–146.

668 Coleman, J. & Spacone, E., 2001. Localization issues in force-based frame elements.
669 *Journal of Structural Engineering,* Volume 127, p. 1257–1265.

670 Coronelli, D. & Gambarova, P., 2004. Structural assessment of corroded reinforced
671 concrete beams: modeling guidelines. *Journal of structural engineering,* Volume 130, p.
672 1214–1224.

673 Dai, K.-Y., Yu, X.-H. & Lu, D.-G., 2020. Phenomenological hysteretic model for corroded
674 RC columns. *Engineering Structures,* Volume 210, p. 110315.

675 Dhakal, R. P. & Maekawa, K., 2002. Modeling for postyield buckling of reinforcement.
676 *Journal of structural engineering,* Volume 128, p. 1139–1147.

677 Dhakal, R. P. & Maekawa, K., 2002. Reinforcement stability and fracture of cover
678 concrete in reinforced concrete members. *Journal of structural engineering,* Volume 128,
679 p. 1253–1262.

680 Du, Y. G., Clark, L. A. & Chan, A. H. C., 2005 (a). Effect of corrosion on ductility of
681 reinforcing bars. *Magazine of Concrete Research,* Volume 57, p. 407–419.

682 Du, Y. G., Clark, L. A. & Chan, A. H. C., 2005 (b). Residual capacity of corroded
683 reinforcing bars. *Magazine of Concrete Research,* Volume 57, p. 135–147.

684 Fardis, M. N. & Biskinis, D. E., 2003. *Deformation capacity of RC members, as controlled*
685 *by flexure or shear.*

Accepted Manuscript

686 Ge, X., Alexander, N. A. & Kashani, M. M., 2020 (b). Rapid post-earthquake damage
687 assessment of ageing reinforced concrete bridge piers using time-frequency analysis.
688 *Structure and Infrastructure Engineering,* p. 1–17.

689 Ge, X., Dietz, M. S., Alexander, N. A. & Kashani, M. M., 2020 (a). Nonlinear dynamic
690 behaviour of severely corroded reinforced concrete columns: shaking table study.
691 *Bulletin of Earthquake Engineering,* Volume 18, p. 1417–1443.

692 Giberson, M. F., 1967. *The response of nonlinear multi-story structures subjected to*
693 *earthquake excitation,*

694 Group, I. T., 2010. *Appraisal of existing structures (Third edition).* s.l.:s.n.

695 Guo, Y., 2011. Assessing the seismic performance of corroding RC bridge columns.

696 Haselton, C. B., 2006. *Assessing seismic collapse safety of modern reinforced concrete*
697 *moment frame buildings.*

698 Haselton, C. B. & Center, P. E. E. R., 2008. *Beam-column element model calibrated for*
699 *predicting flexural response leading to global collapse of RC frame buildings.* Pacific
700 Earthquake Engineering Research Center.

701 Haselton, C. B. et al., 2008. An assessment to benchmark the seismic performance of a
702 code-conforming reinforced-concrete moment-frame building. *Pacific Earthquake*
703 *Engineering Research Center.*

704 Haselton, C. B., Liel, A. B., Taylor-Lange, S. C. & Deierlein, G. G., 2016. Calibration of
705 model to simulate response of reinforced concrete beam-columns to collapse.. *ACI*
706 *Structural Journal,* Volume 113.

707 Ibarra, L. F., Medina, R. A. & Krawinkler, H., 2005. Hysteretic models that incorporate
708 strength and stiffness deterioration. *Earthquake engineering & structural dynamics,*
709 Volume 34, p. 1489–1511.

Accepted Manuscript

Johnson, N., 2006. *Large-scale experimental and analytical seismic studies of a two-span reinforced concrete bridge system.* s.l.:University of Nevada, Reno.

Kashani, M. M., Crewe, A. J. & Alexander, N. A., 2013. Use of a 3D optical measurement technique for stochastic corrosion pattern analysis of reinforcing bars subjected to accelerated corrosion. *Corrosion Science,* Volume 73, p. 208–221.

Kashani, M. M., Lowes, L. N., Crewe, A. J. & Alexander, N. A., 2014. Finite element investigation of the influence of corrosion pattern on inelastic buckling and cyclic response of corroded reinforcing bars. *Engineering Structures,* Volume 75, p. 113–125.

Kashani, M. M., Lowes, L. N., Crewe, A. J. & Alexander, N. A., 2015. Phenomenological hysteretic model for corroded reinforcing bars including inelastic buckling and low-cycle fatigue degradation. *Computers & Structures,* Volume 156, p. 58–71.

Kashani, M. M., Lowes, L. N., Crewe, A. J. & Alexander, N. A., 2016. Nonlinear fibre element modelling of RC bridge piers considering inelastic buckling of reinforcement. *Engineering Structures,* Volume 116, p. 163–177.

Kunnath, S. K., Reinhorn, A. M. & Park, Y. J., 1990. Analytical modeling of inelastic seismic response of R/C structures. *Journal of Structural Engineering,* Volume 116, p. 996–1017.

Lehman, D. E., 2000. Seismic performance of well-confined concrete bridge columns..

Lignos, D., 2008. *Sidesway collapse of deteriorating structural systems under seismic excitations.* s.l.:Stanford university.

Lignos, D. G. & Krawinkler, H., 2011. Deterioration modeling of steel components in support of collapse prediction of steel moment frames under earthquake loading. *Journal of Structural Engineering,* Volume 137, p. 1291–1302.

Accepted Manuscript

Li, T., Lin, J. & Liu, J., 2020. *Analysis of time-dependent seismic fragility of the offshore bridge under the action of scour and chloride ion corrosion.* s.l., s.n., p. 1785–1801.

Lundgren, K., 2007. Effect of corrosion on the bond between steel and concrete: an overview. *Magazine of Concrete Research,* Volume 59, p. 447–461.

Mahadik, V. et al., n.d. Behavior of Corroded Reinforced Concrete Beams under Flexure-Numerical Simulation.

Mayes, R. L. & Friedland, I. M., 2002. *Recommended LRFD Guidelines for the seismic design of highway bridges.* s.l., s.n.

McKenna, F., 2011. OpenSees: a framework for earthquake engineering simulation. *Computing in Science & Engineering,* Volume 13, p. 58–66.

Meda, A., Mostosi, S., Rinaldi, Z. & Riva, P., 2014. Experimental evaluation of the corrosion influence on the cyclic behaviour of RC columns. *Engineering Structures,* Volume 76, p. 112–123.

Menegotto, M., 1973. *Method of analysis for cyclically loaded RC plane frames including changes in geometry and non-elastic behavior of elements under combined normal force and bending.* s.l., s.n., p. 15–22.

Moyer, M. J. & Kowalsky, M. J., 2003. Influence of tension strain on buckling of reinforcement in concrete columns. *ACI Structural journal,* Volume 100, p. 75–85.

Mo, Y.-L. & Wang, S. J., 2000. Seismic behavior of RC columns with various tie configurations. *Journal of Structural Engineering,* Volume 126, p. 1122–1130.

Otani, S., 1974. Inelastic analysis of R/C frame structures. *Journal of the Structural Division,* Volume 100, p. 1433–1449.

Panagiotakos, T. B. & Fardis, M. N., 2001. Deformations of reinforced concrete members at yielding and ultimate. *Structural Journal,* Volume 98, p. 135–148.

Accepted Manuscript

Parke, G. A. & Hewson, N., 2008. *ICE Manual of Bridge Engineering.*

Ramberg, W. & Osgood, W. R., 1943. Description of stress-strain curves by three parameters.

Rao, A. S., Lepech, M. D., Kiremidjian, A. S. & Sun, X.-Y., 2017. Simplified structural deterioration model for reinforced concrete bridge piers under cyclic loading. *Structure and Infrastructure Engineering,* Volume 13, p. 55–66.

Roohbakhsh, H. & Kalantari, A., 2018. *Seismic performance assessment of RC structures exposed to the corrosion aggressive environment of the Persian Gulf.* s.l., s.n.

Scott, B. D., 1982. Park. *R and Priestley. MJ N_{S}{t}{r}ee—strain Behavior of Concrete Confined by Overlapping H0ops at and HigII Strain Rates. Joum81 of The American Concrete Institute,* Volume 79, p. 13–27.

Sharma, A. et al., 2012. Behavior of Corroded Reinforced Concrete Beams under Flexure-Numerical Simulation.

Song, J.-K. & Pincheira, J., 2000. Spectral displacement demands of stiffness-and strength-degrading systems. *Earthquake Spectra,* Volume 16, p. 817–851.

Stratfull, R. F., 1957. The corrosion of steel in a reinforced concrete bridge. *Corrosion,* Volume 13, p. 43–48.

Takizawa, H. A. R. U. O., 1976. Notes on some basic problems in inelastic analysis of planar R/C structures (part i). *Transactions of the Architectural Institute of Japan,* Volume 240, p. 51–62.

Taucer, F., Spacone, E. & Filippou, F. C., 1991. *A fiber beam-column element for seismic response analysis of reinforced concrete structures.* s.l.:Earthquake Engineering Research Center, College of Engineering, University ….

Accepted Manuscript

780 Taucer, F., Spacone, E. & Filippou, F. C., 1991. *A fiber beam-column element for seismic*
781 *response analysis of reinforced concrete structures.* s.l.:Earthquake Engineering
782 Research Center, College of Engineering, University ….

783 Tuutti, K., 1982. *Corrosion of steel in concrete.* s.l.:Cement-och betonginst..

784 Vu, K. A. T. & Stewart, M. G., 2000. Structural reliability of concrete bridges including
785 improved chloride-induced corrosion models. *Structural safety,* Volume 22, p. 313–333.

786 Wang, C.-h., Foliente, G. C., Sivaselvan, M. V. & Reinhorn, A. M., 2001. Hysteretic
787 models for deteriorating inelastic structures. *Journal of Engineering Mechanics,* Volume
788 127, p. 1200–1202.

789 Yang, J., Guo, T. & Chai, S., 2020. *Experimental and numerical investigation on seismic*
790 *behaviours of beam-column joints of precast prestressed concrete frame under given*
791 *corrosion levels.* s.l., s.n., p. 1209–1221.

792 Yang, S.-Y.et al., 2016. Experimental research on hysteretic behaviors of corroded
793 reinforced concrete columns with different maximum amounts of corrosion of rebar.
794 *Construction and Building Materials,* Volume 121, p. 319–327.

795 Yu, R., Chen, L., Zhang, D. & Wang, Z., 2020. *Life cycle embodied energy analysis of*
796 *RC structures considering chloride-induced corrosion in seismic regions.* s.l., s.n., p.
797 839–848.

798 Zadeh, M. S. & Saiidi, M. S., 2007. Pre-test analytical studies of NEESR-SG 4-span
799 bridge model using OpenSees. *Rep. No. CCEER-07,* Volume 3.

800 Zhao, J. & Sritharan, S., 2007. Modeling of strain penetration effects in fiber-based
801 analysis of reinforced concrete structures. *ACI Materials Journal,* Volume 104, p. 133.

802

803

Accepted Manuscript

804 **Tables**

805 Table 1. Details of considered column elements for verifying the mentioned FE model

	ψ	ν	ρ_v	$f_c^{'}$	f_y	ρ_h	f_u	f_{yh}
Mo et. al.	0	0.113	0.0214	24.9	497	0.011	592	459.5
(Meda, et al., 2014) (UC)	0	0.22	0.0089	20	520	0.0045	620	520
(Meda, et al., 2014) (C)	20	0.22	0.0089	20	520	0.0045	620	520
(Moyer & Kowalsky, 2003) (#1)	0	0.041	0.0198	32.7	565.4	0.0092	696.4	434.4
(Lehman, 2000) (415)	0	0.072	0.0149	31	462	0.007	630	606.8

806

807

808 Table 2. Details of RC columns in the simulation data from parametric study

axial load ratio (N/Agfc)		0.05	0.1	0.2	0.3			
longitudinal reinforcement ratio (%)		1	1.5	2	2.5	3		
concrete strength (Mpa)		20	30	40	50			
reinforcement Properties	Ultimate (MPa)	500	600	650				
	Yield (MPa)	340	400	500				
transverse reinforcement ratio (%)		0.16	0.3	0.6	0.9			
corrosion (%)		0	4	8	12	16	20	24

809

810 Table 3. Monotonic parameters in the modified Ibarra-Krawinkler model (Lignos, 2008)

Monotonic parameters			
Parameter	Description	Parameter	Description
K_0	elastic stiffness	θ_{pc}^{+}	post-capping rotation for positive loading direction
α_s^{+}	strain hardening ratio for positive loading direction	θ_{pc}^{-}	post-capping rotation for negative loading direction
α_s^{-}	strain hardening ratio for negative loading direction	θ_u^{+}	ultimate rotation capacity for positive loading direction
M_y^{+}	effective yield strength for positive loading direction	θ_u^{-}	ultimate rotation capacity for negative loading direction
M_y^{-}	effective yield strength for negative loading direction	r^{+}	residual strength ratio for positive loading direction
θ_p^{+}	pre-capping rotation for positive loading direction	r^{-}	residual strength ratio for negative loading direction
θ_p^{-}	pre-capping rotation for negative loading direction		

811

812

Accepted Manuscript

Table 4. Cyclic parameters in the modified Ibarra-Krawinkler model (Lignos, 2008)

Cyclic parameters			
Parameter	Description	Parameter	Description
λ_s	Cyclic deterioration parameter for strength deterioration	C_c	rate of post-capping strength deterioration
λ_c	Cyclic deterioration parameter for post-capping strength deterioration	C_A	rate of accelerated reloading deterioration
λ_A	Cyclic deterioration parameter for accelerated reloading stiffness deterioration	C_k	rate of unloading stiffness deterioration
λ_k	Cyclic deterioration parameter for unloading stiffness deterioration	D^+	rate of cyclic deterioration in the positive loading direction
C_s	rate of strength deterioration	D^-	rate of cyclic deterioration in the negative loading direction

Table 5. Details of No. 411 column which used for calibrating λ

	ψ	ν	ρ_v	$f_c^{'}$	f_y	ρ_h	f_u	f_{yh}
Column #411	0	0.1	0.025	40	340	0.006	500	340

Table 6. Statistical specifications of parameters for circular and rectangular models

		mean	Median	Standard deviation	R-squared factor
Rectangular columns	θ_y	1.009	1.013	0.108	88
	M_y	1.001	0.997	0.097	94
	θ_p	1.012	1.007	0.165	85
	M_p	1.020	0.992	0.202	91
	θ_{pc}	1.034	1.011	0.241	80
Circular columns	θ_y	1.004	0.997	0.063	95
	M_y	1.002	0.997	0.095	93
	θ_p	1.023	1.019	0.149	86
	M_p	1.004	0.997	0.085	93
	θ_{pc}	1.039	1.049	0.170	84

Accepted Manuscript

Table 7. Details of considered column elements for verifying the proposed hinge models

		ψ	ν	ρ_v	$f_c^{'}$	f_y	ρ_h	f_u	f_{yh}
Rectangular	R1	0	0.07	0.022	45	480	0.006	635	400
	R2	6	0.07	0.022	45	480	0.006	635	380
	R3	15	0.05	0.021	42	450	0.006	610	400
	R4	22	0.06	0.020	43	460	0.007	620	400
	R5	3	0.15	0.029	55	320	0.009	480	400
	R6	8	0.10	0.03	48	490	0.01	640	550
Circular	C1	0	0.20	0.020	20	460	0.003	620	400
	C2	6	0.05	0.025	32	340	0.003	500	400
	C3	11	0.05	0.012	30	470	0.007	610	400
	C4	18	0.05	0.018	33	500	0.007	650	400
	C5	22	0.05	0.020	37	340	0.005	500	340

Table 8. column of Johnson's bridge model properties and corresponding plastic hinge model details (Johnson, 2006)

Design parameters	ψ	ν	ρ_v	$f_c^{'}$	f_y	ρ_h	f_u	f_{yh}
	0	0.08	0.0156	40.7	462	0.009	552	462
Plastic hinge properties	θ_y	M_y (kN-m)	θ_p	M_p (kN-m)	θ_{pc}	λ		
	0.0079	184.9	0.038	188.8	0.0477	3.01		

Table 9. comparison between calculated and experimental modal properties

		1st mode	**2nd mode**	**3rd mode**	**4th mode**
Time period (s)	Johnson's Study (Johnson, 2006)	0.44	0.37	0.30	0.20
	Current study FE model	0.48	0.43	0.35	0.23
Frequencies (Hz)	Johnson's Study (Johnson, 2006)	2.29	2.73	3.37	4.88
	Current study FE model	2.08	2.33	2.86	4.35

Accepted Manuscript

Figure captions

Figure 1. An example of bridge pier which is mentioned in this study, Ehsan intersection bridge, Shiraz

Figure 2. Finite element model and fibre section schematics for circular and rectangular RC columns

Figure 3. Comparison between results of presented FE model and experimental studies (a) (Mo & Wang, 2000) (C1-1), (b) (Meda, et al., 2014) (uncorroded), (c) (Meda, et al., 2014) (corroded), (d) (Moyer & Kowalsky, 2003) (No. 1 column), (e) (Lehman, 2000) (column 415)

Figure 4. Ibarra's lumped plasticity model (Ibarra, et al., 2005)

Figure 5. Basic parameters of modified Ibarra-Krawinkler model (Lignos, 2008)

Figure 6. Cyclic and monotonic result of No. 411 column analysis

Figure 7. Calibration procedure of λ for No. 411 rectangular RC column, (a) λ =2.00, (b) λ =2.25, (c) λ =2.5, (d) λ =2.75, (e) λ =3, (f) λ =3.25, (g) λ =3.50, (h) λ =3.75

Figure 8. Effect of corrosion and axial load on the calibrated parameters, (a) Yield rotation, (b) Yield moment, (c) Capping rotation, (d) Capping moment, (e) Post-capping rotation

Figure 9: Effect of corrosion and longitudinal bar ratio on the calibrated parameters, (a) Yield rotation, (b) Yield moment, (c) Capping rotation, (d) Capping moment, (e) Post-capping rotation

Figure 10: Effect of corrosion and Concrete compressive strength on the calibrated parameters, (a) Yield rotation, (b) Yield moment, (c) Capping rotation, (d) Capping moment, (e) Post-capping rotation

Figure 11. dependency between moment and rectangular cross sections, (a) Yield moment, (b) Capping moment

Figure 12. dependency between moment and circular cross sections, (a) Yield moment, (b) Capping moment

Figure 13. Capping rotation for all circular columns

Accepted Manuscript

Figure 14. Comparison between predicted and true responses for rectangular columns, (a) yield rotation, (b) yield moment, (c) capping rotation, (d) capping moment, (e) post-capping rotation

Figure 15. Comparison between predicted and true responses for circular columns, (a) yield rotation, (b) yield moment, (c) capping rotation, (d) capping moment, (e) post-capping rotation

Figure 16. ACI-374 cyclic load pattern (ACI Committee, 2005)

Figure 17. Results of proposed model and finite element fiber model (rectangular), (a) R1, (b)R2 (c)R3, (d)R4, (e)R5, (f)R6

Figure 18. Comparison between results of predicted model and finite element fiber model (circular), (a) C1, (b) C2, (c) C3, (d) C4, (e) C5

Figure 19. Comparison between results of predicted model and experimental studies, (a) (Mo & Wang, 2000) (C1-1), (b) (Meda, et al., 2014) (uncorroded), (c) (Meda, et al., 2014) (corroded), (d) (Moyer & Kowalsky, 2003) (No. 1 column), (e) (Lehman, 2000) (column 415)

Figure 20. Bridge model descriptions (Johnson, 2006), (a) 3D prototype, (b) Opensees FE prototype model (c) longitudinal side view, (d) transvers side view, (e) columns section properties, (f) detail of bridge foundation

Figure 21. measured displacement of shake table (test #16) (Johnson, 2006)

Figure 22. comparison between calculated and experimental time history results (test #14)

Figure 23. comparison between calculated and experimental time history results (test #16)

Figure 24. comparison between calculated and experimental time history results (test #18)

Accepted Manuscript

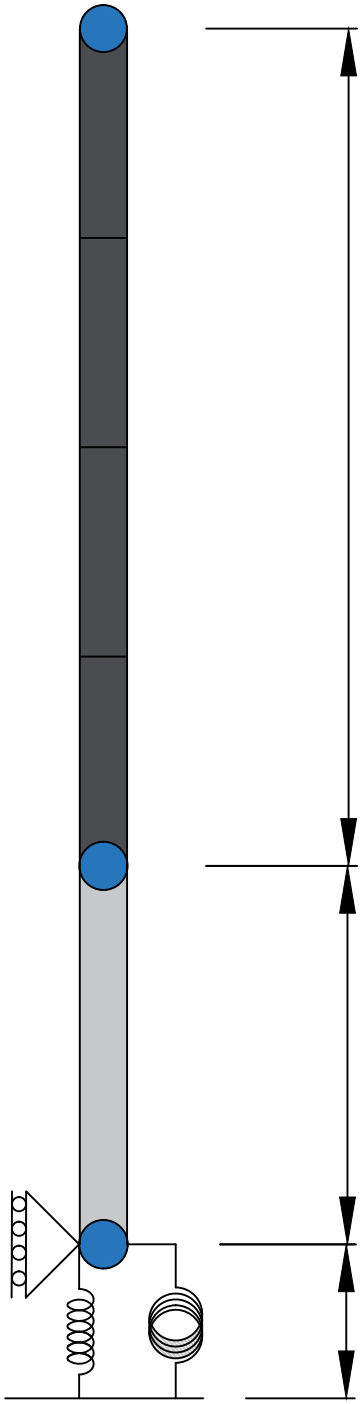

Second element
five integration points
L2=L-L1

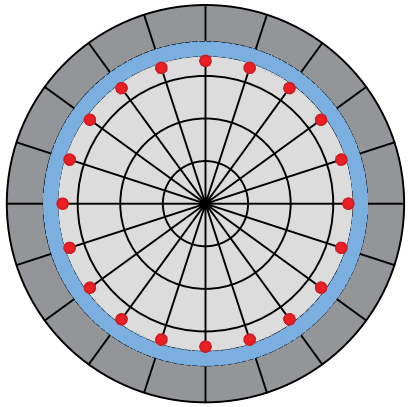

First element
Rectangular:
two integration points (L1=2*Leff)

Circular:
three integration points (L1=6*Leff)

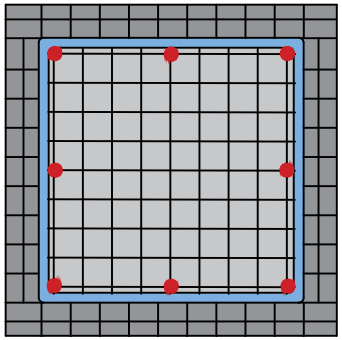

Zero length section element

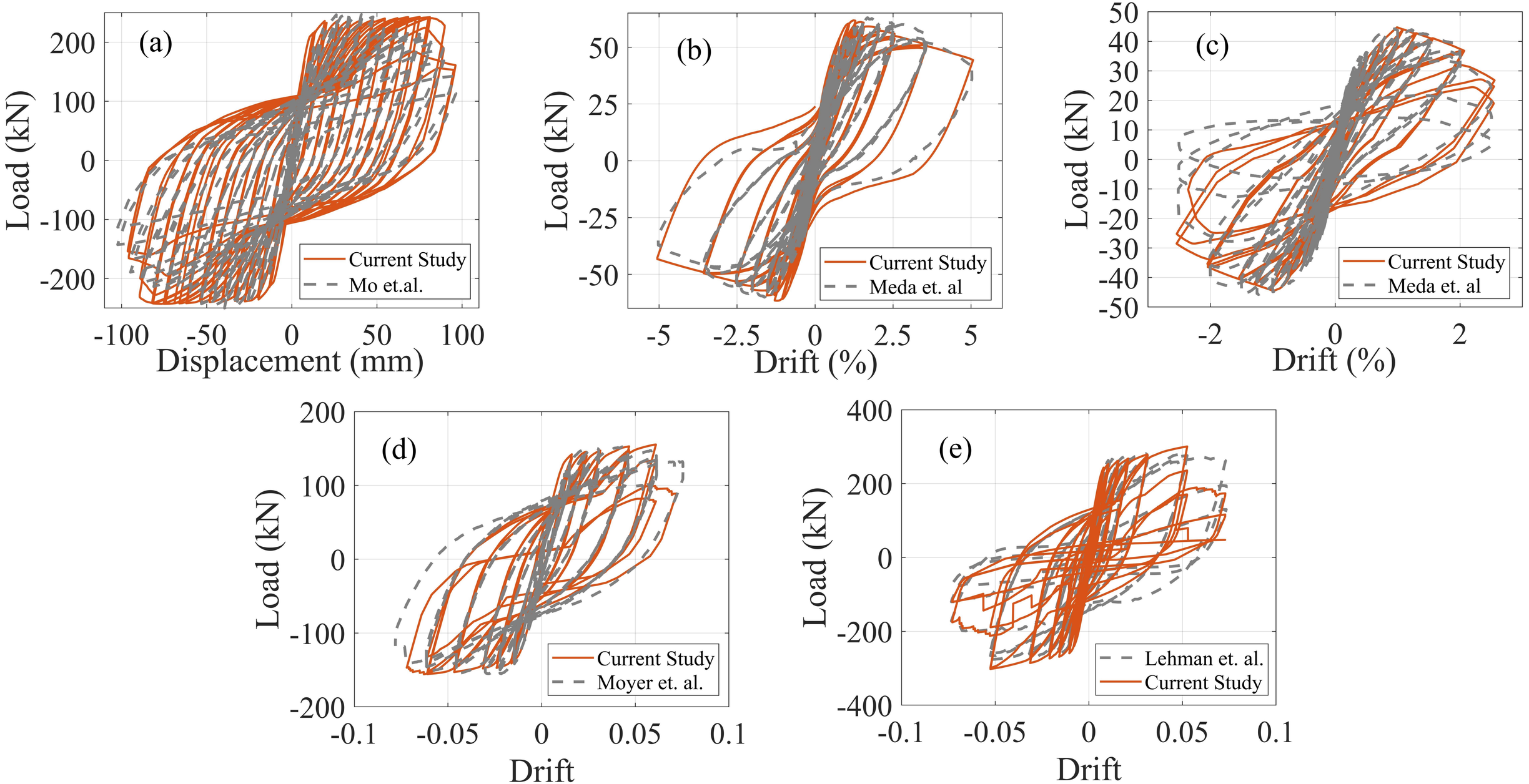
(a)
Load (kN)
Displacement (mm)
Current Study
Mo et.al.
(b)
Load (kN)
Drift (%)
Current Study
Meda et. al
(c)
Load (kN)
Drift (%)
Current Study
Meda et. al
(d)
Load (kN)
Drift
Current Study
Moyer et. al.
(e)
Load (kN)
Drift
Lehman et. al.
Current Study

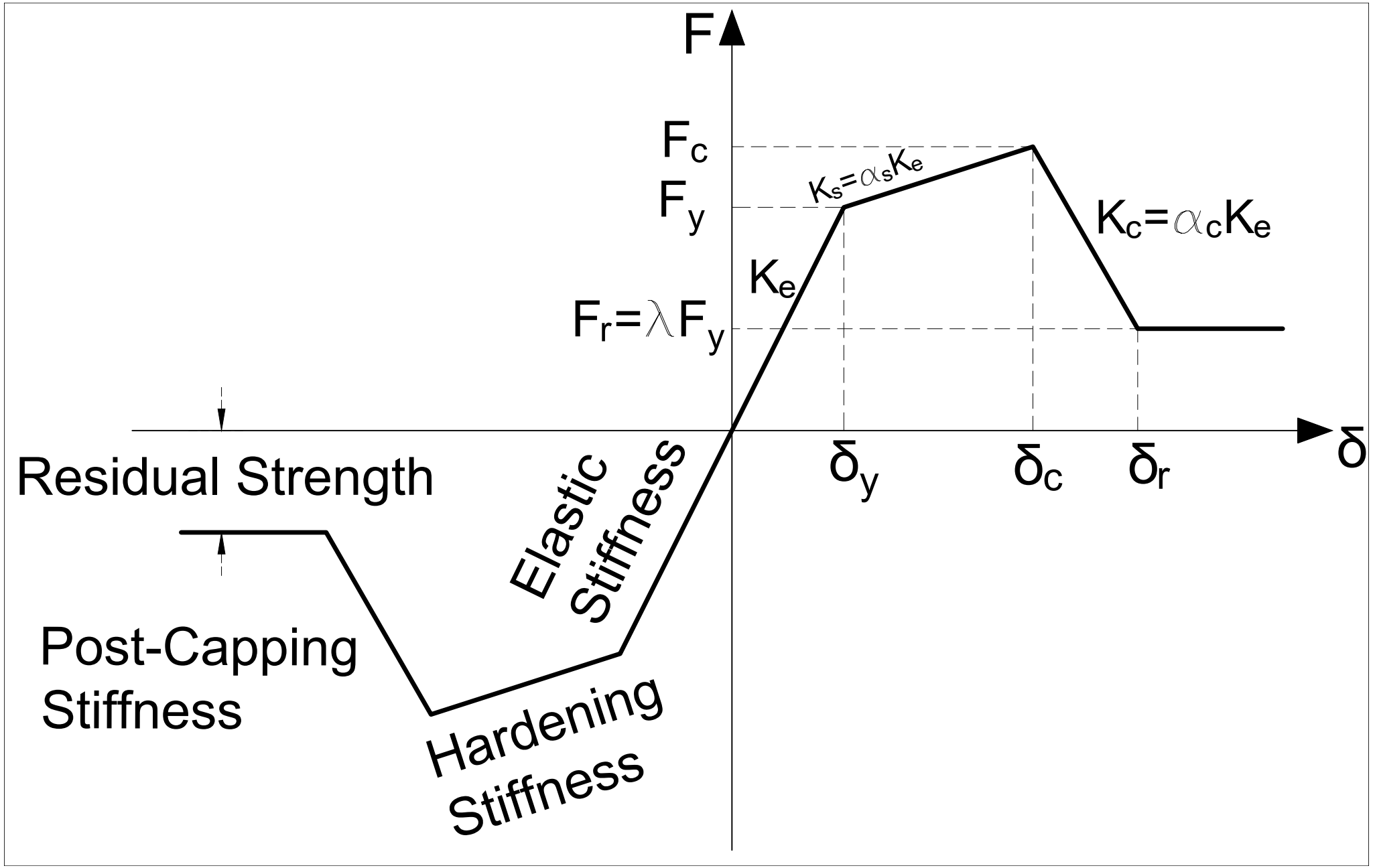
F
Fc
Fy
Ke
Fr=λFy
Ks=αsKe
Kc=αcKe
δy
δc
δr
δ
Residual Strength
Elastic Stiffness
Post-Capping Stiffness
Hardening Stiffness

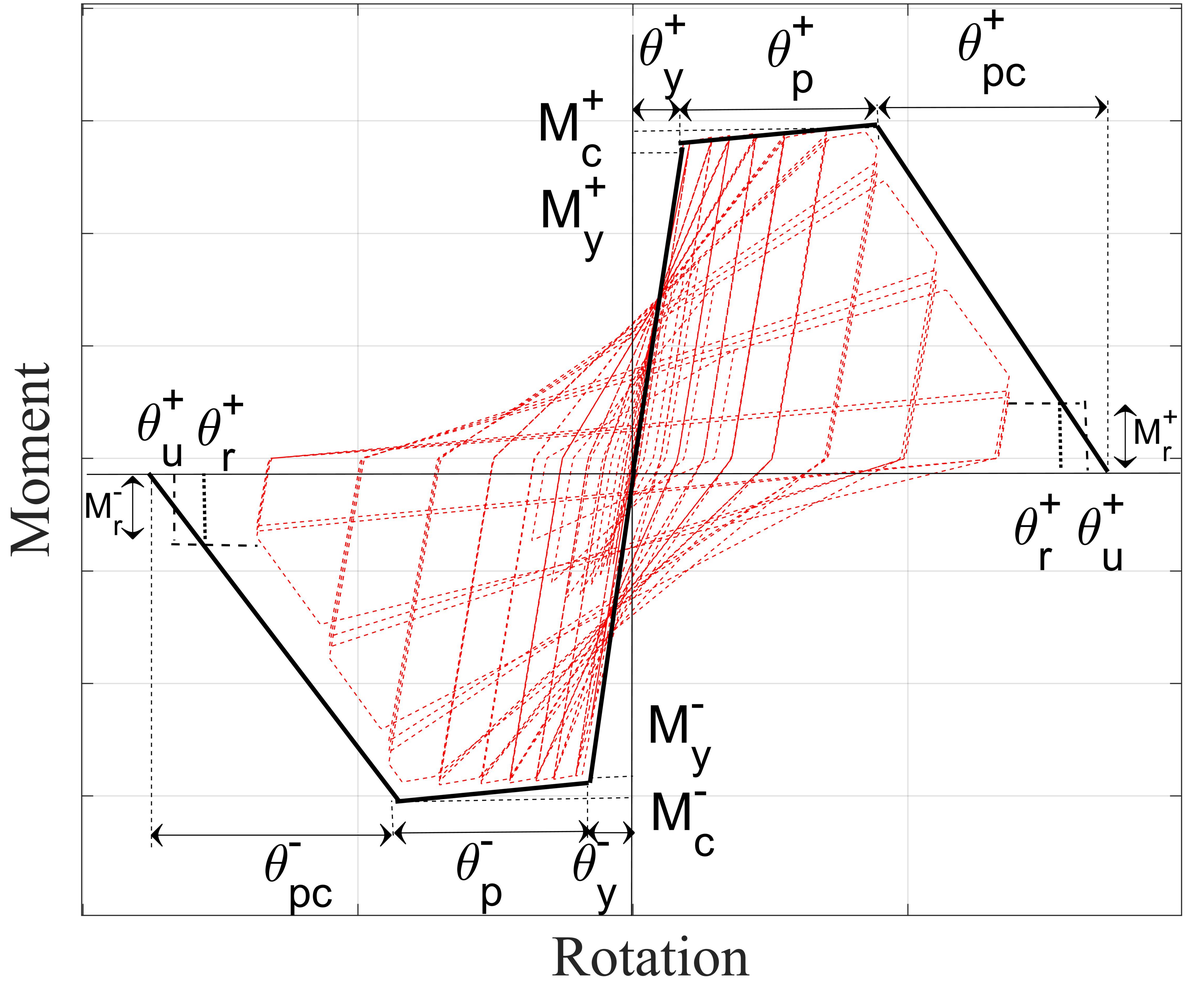
Moment
Rotation
θ^+_y
θ^+_p
θ^+_{pc}
M^+_c
M^+_y
θ^+_u θ^+_r
M^+_r
M^-_r
θ^+_r θ^+_u
M^-_y
M^-_c
θ^-_{pc}
θ^-_p
θ^-_y

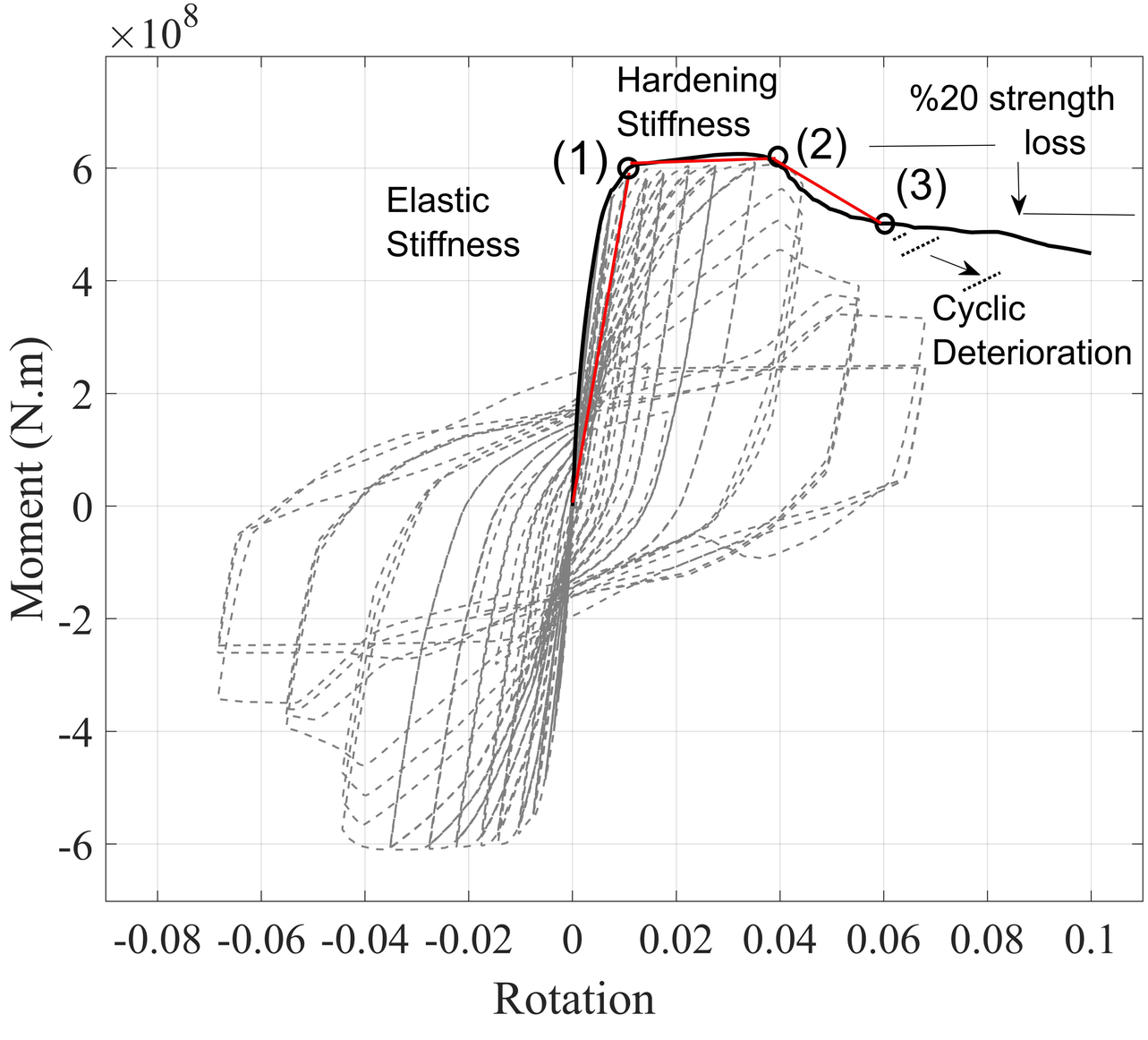
×10^8
Hardening
Stiffness
(1)
(2)
(3)
%20 strength
loss
Elastic
Stiffness
Cyclic
Deterioration
Moment (N.m)
Rotation
6
4
2
0
-2
-4
-6
-0.08
-0.06
-0.04
-0.02
0
0.02
0.04
0.06
0.08
0.1

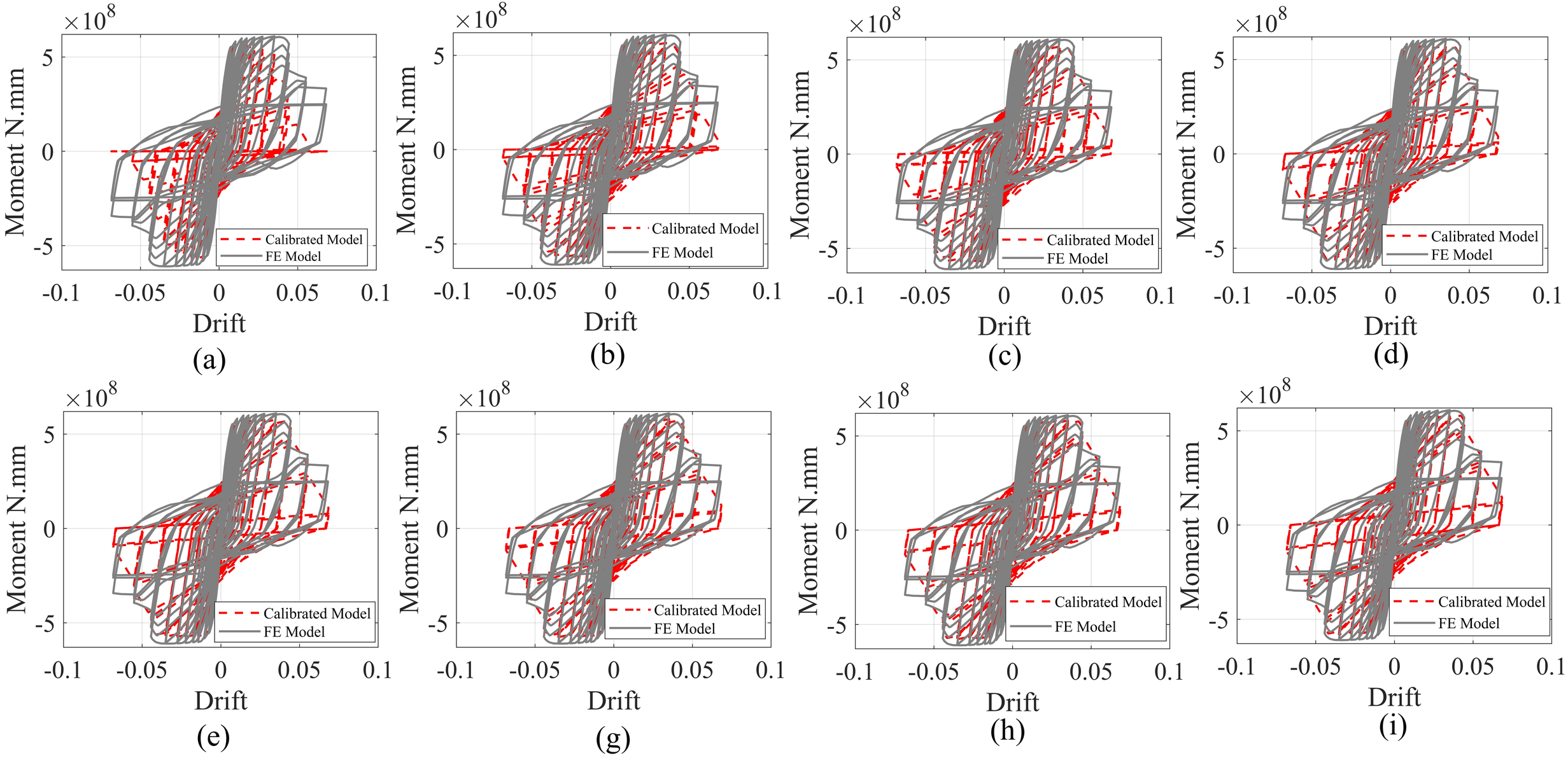
×10^8
Moment N.mm
Drift
Calibrated Model
FE Model
(a)
(b)
(c)
(d)
(e)
(g)
(h)
(i)

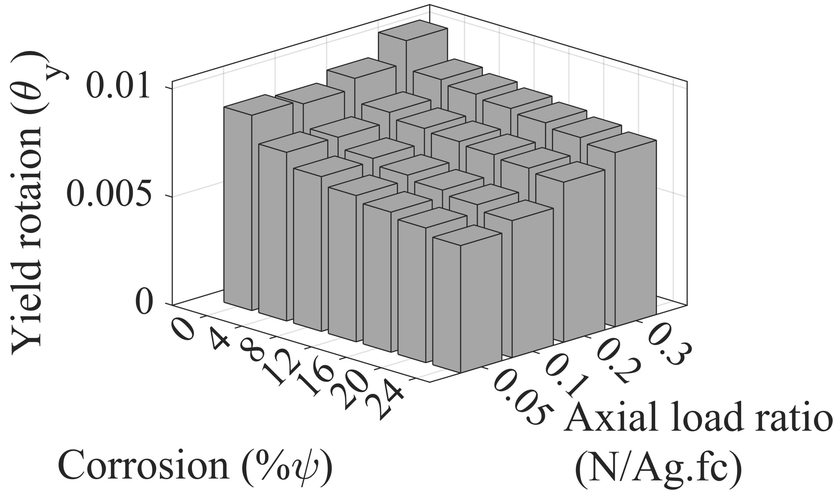
Yield rotaion (θ_y)
0.01
0.005
0
0 4 8 12 16 20 24
Corrosion (%ψ)
0.05 0.1 0.2 0.3
Axial load ratio
(N/Ag.fc)

(a)

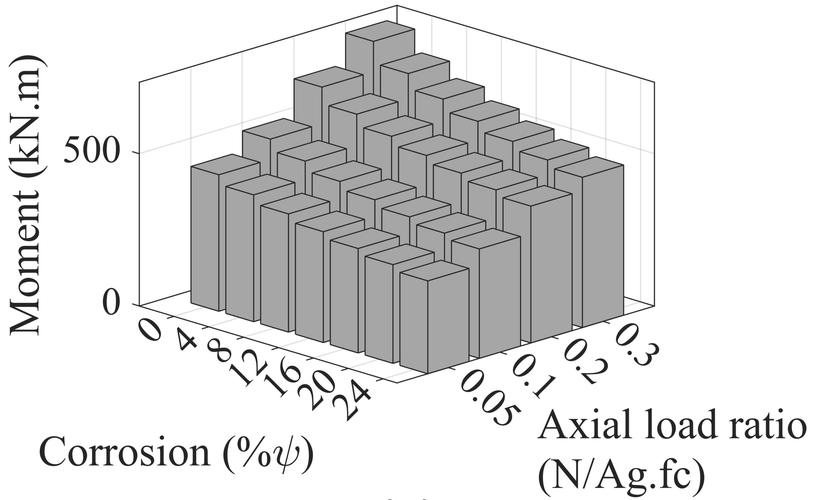
Moment (kN.m)
500
0
0 4 8 12 16 20 24
Corrosion (%ψ)
0.05 0.1 0.2 0.3
Axial load ratio
(N/Ag.fc)

(b)

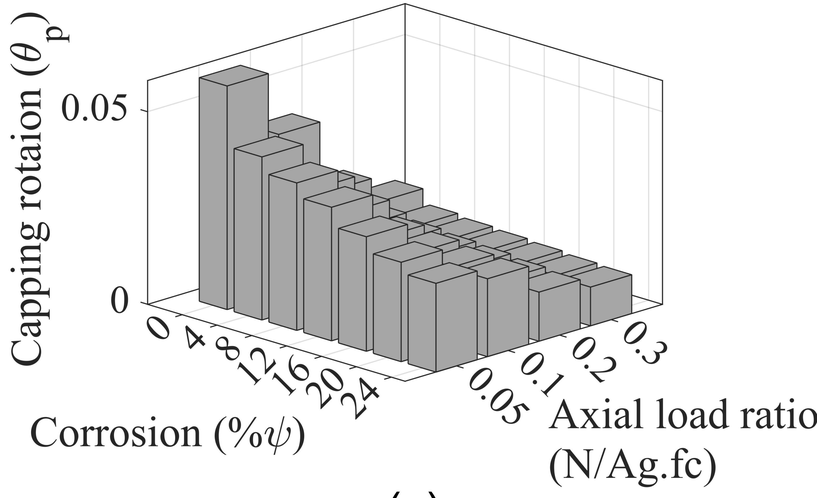
Capping rotaion (θ_p)
0.05
0
0 4 8 12 16 20 24
Corrosion (%ψ)
0.05 0.1 0.2 0.3
Axial load ratio
(N/Ag.fc)

(c)

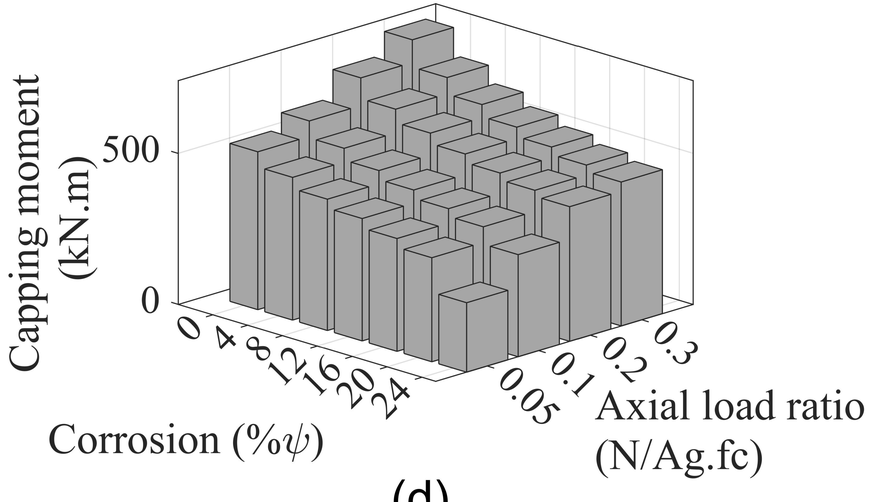
Capping moment
(kN.m)
500
0
0 4 8 12 16 20 24
Corrosion (%ψ)
0.05 0.1 0.2 0.3
Axial load ratio
(N/Ag.fc)

(d)

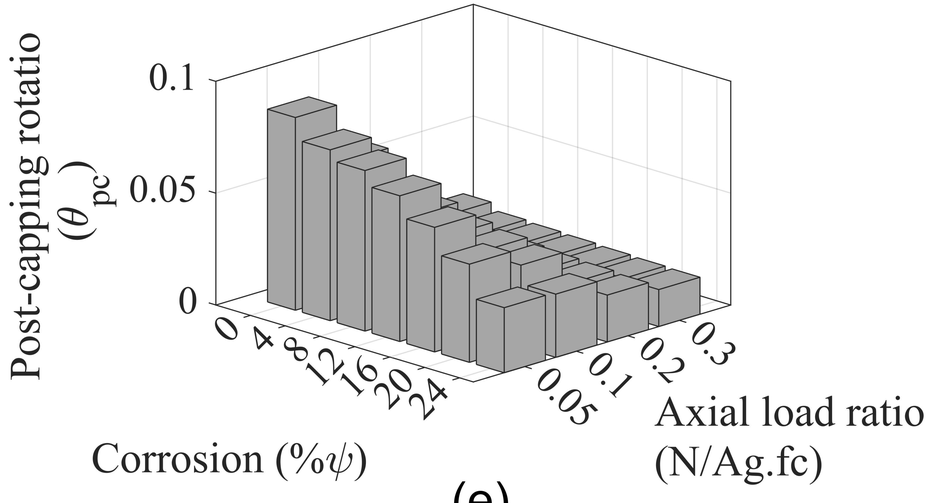
Post-capping rotatio
(θ_{pc})
0.1
0.05
0
0 4 8 12 16 20 24
Corrosion (%ψ)
0.05 0.1 0.2 0.3
Axial load ratio
(N/Ag.fc)

(e)

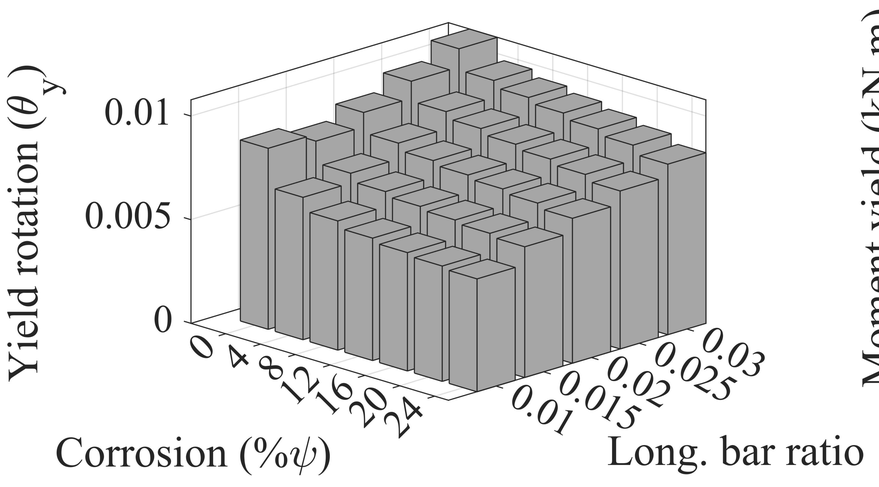
Yield rotation (θ_y)
0.01
0.005
0
0 4 8 12 16 20 24
Corrosion (%ψ)
0.01 0.015 0.02 0.025 0.03
Long. bar ratio

(a)

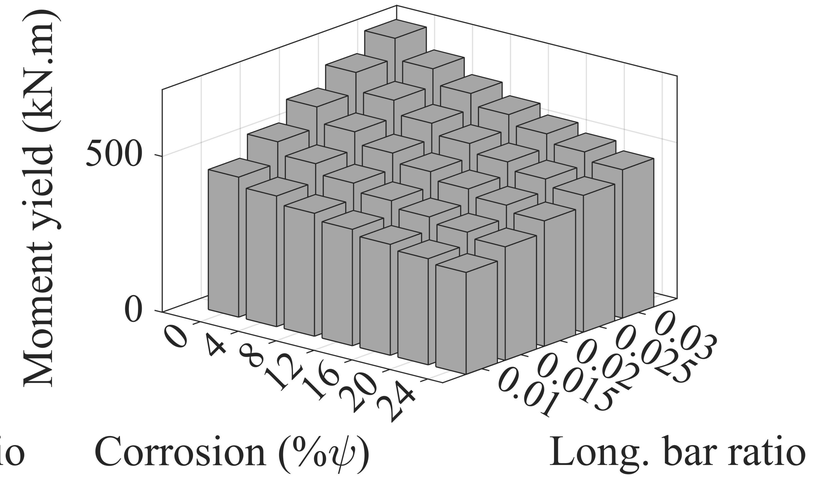
Moment yield (kN.m)
500
0
0 4 8 12 16 20 24
Corrosion (%ψ)
0.01 0.015 0.02 0.025 0.03
Long. bar ratio

(b)

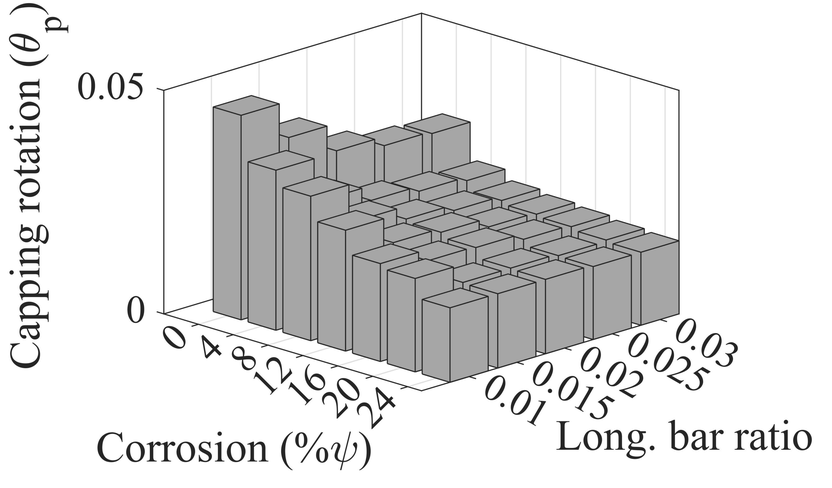
Capping rotation (θ_p)
0.05
0
0 4 8 12 16 20 24
Corrosion (%ψ)
0.01 0.015 0.02 0.025 0.03
Long. bar ratio

(c)

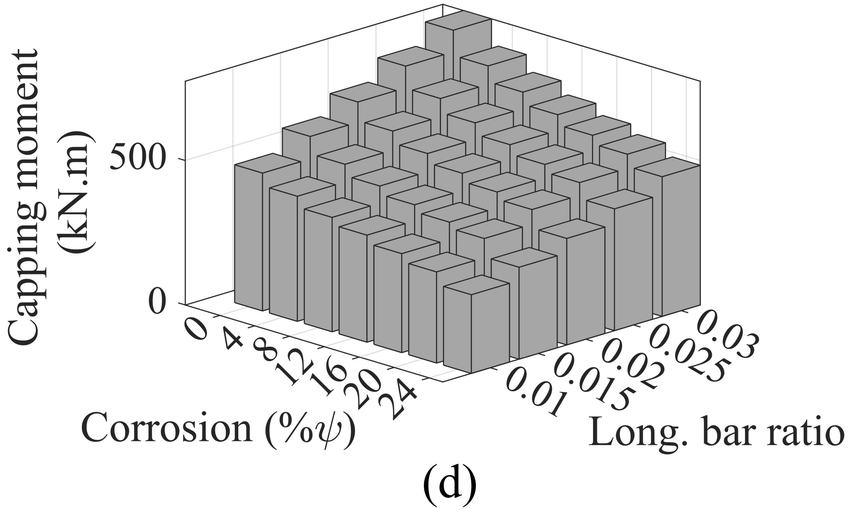
Capping moment (kN.m)
500
0
0 4 8 12 16 20 24
Corrosion (%ψ)
0.01 0.015 0.02 0.025 0.03
Long. bar ratio

(d)

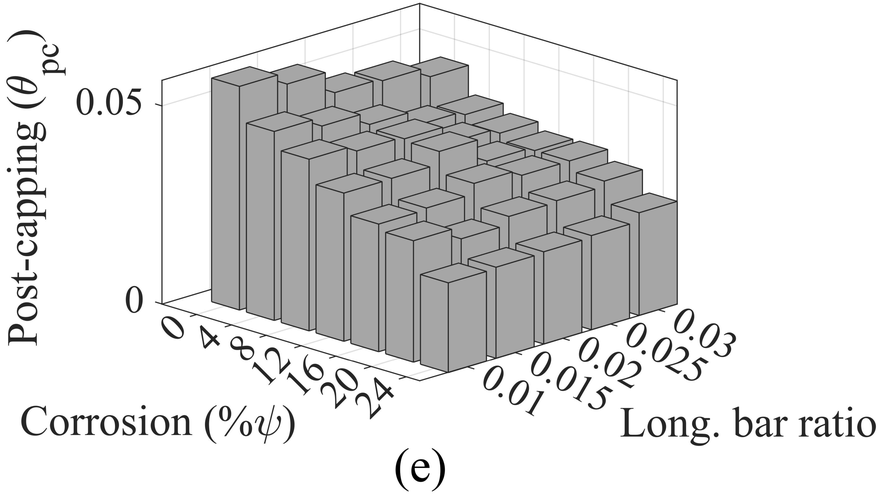
Post-capping (θ_{pc})
0.05
0
0 4 8 12 16 20 24
Corrosion (%ψ)
0.01 0.015 0.02 0.025 0.03
Long. bar ratio

(e)

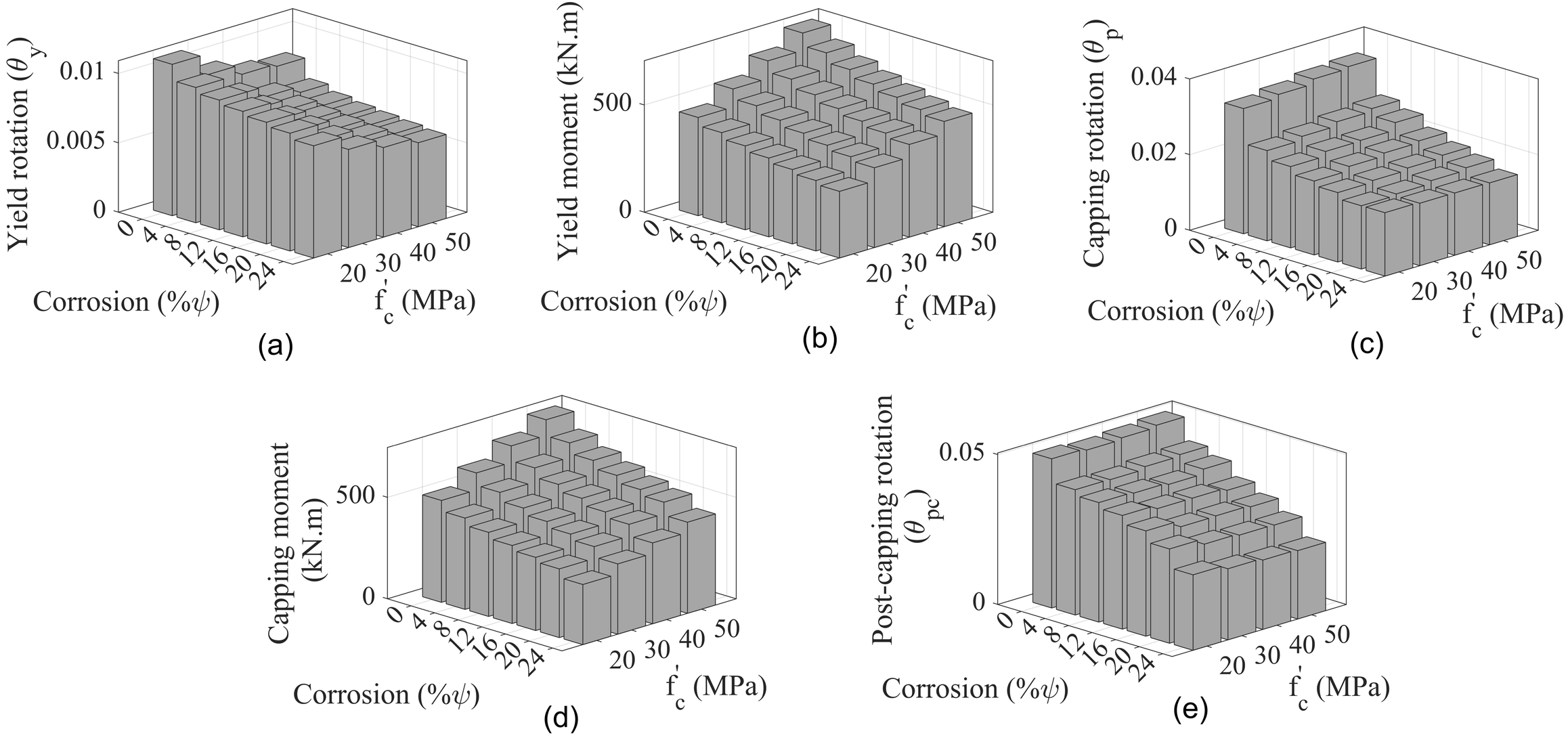
Yield rotation (θ_y)
0.01
0.005
0
0 4 8 12 16 20 24
Corrosion (%ψ)
20 30 40 50
f_c' (MPa)
(a)
Yield moment (kN.m)
500
0
0 4 8 12 16 20 24
Corrosion (%ψ)
20 30 40 50
f_c' (MPa)
(b)
Capping rotation (θ_p)
0.04
0.02
0
0 4 8 12 16 20 24
Corrosion (%ψ)
20 30 40 50
f_c' (MPa)
(c)
Capping moment (kN.m)
500
0
0 4 8 12 16 20 24
Corrosion (%ψ)
20 30 40 50
f_c' (MPa)
(d)
Post-capping rotation (θ_{pc})
0.05
0
0 4 8 12 16 20 24
Corrosion (%ψ)
20 30 40 50
f_c' (MPa)
(e)

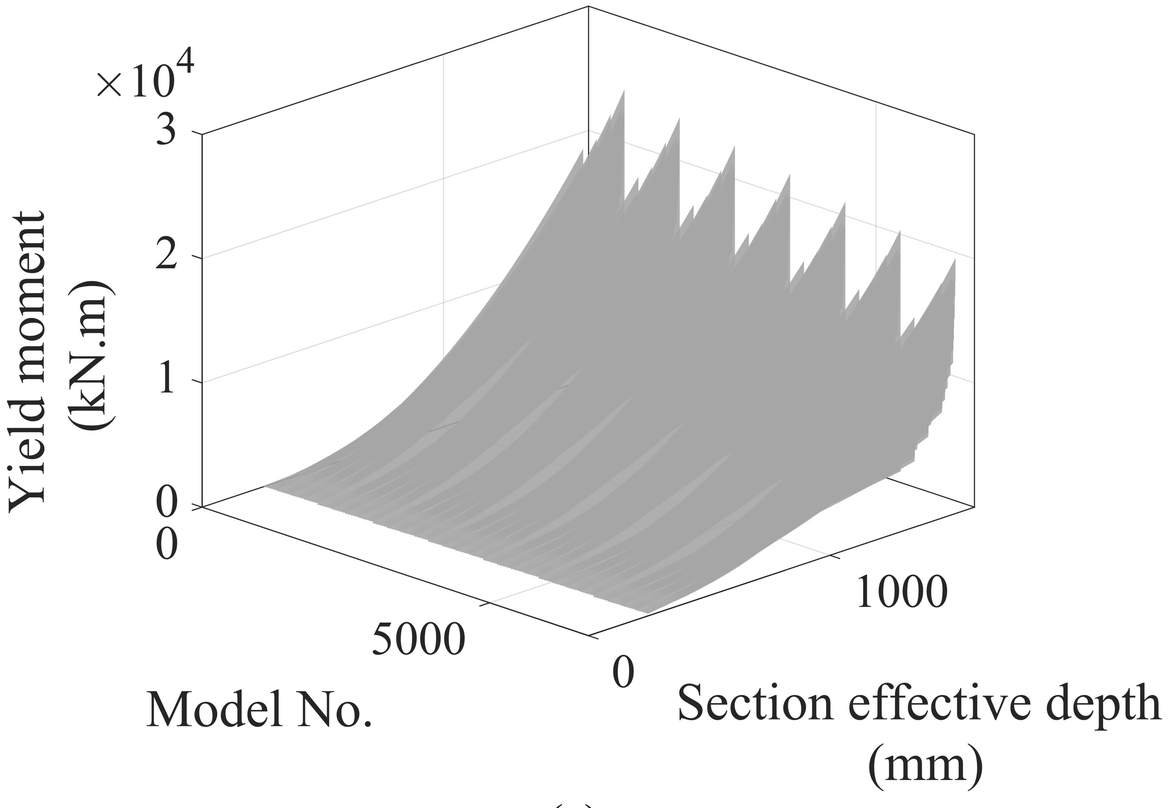
×10^4
3
2
1
0
Yield moment
(kN.m)
0
5000
Model No.
0
1000
Section effective depth
(mm)

(a)

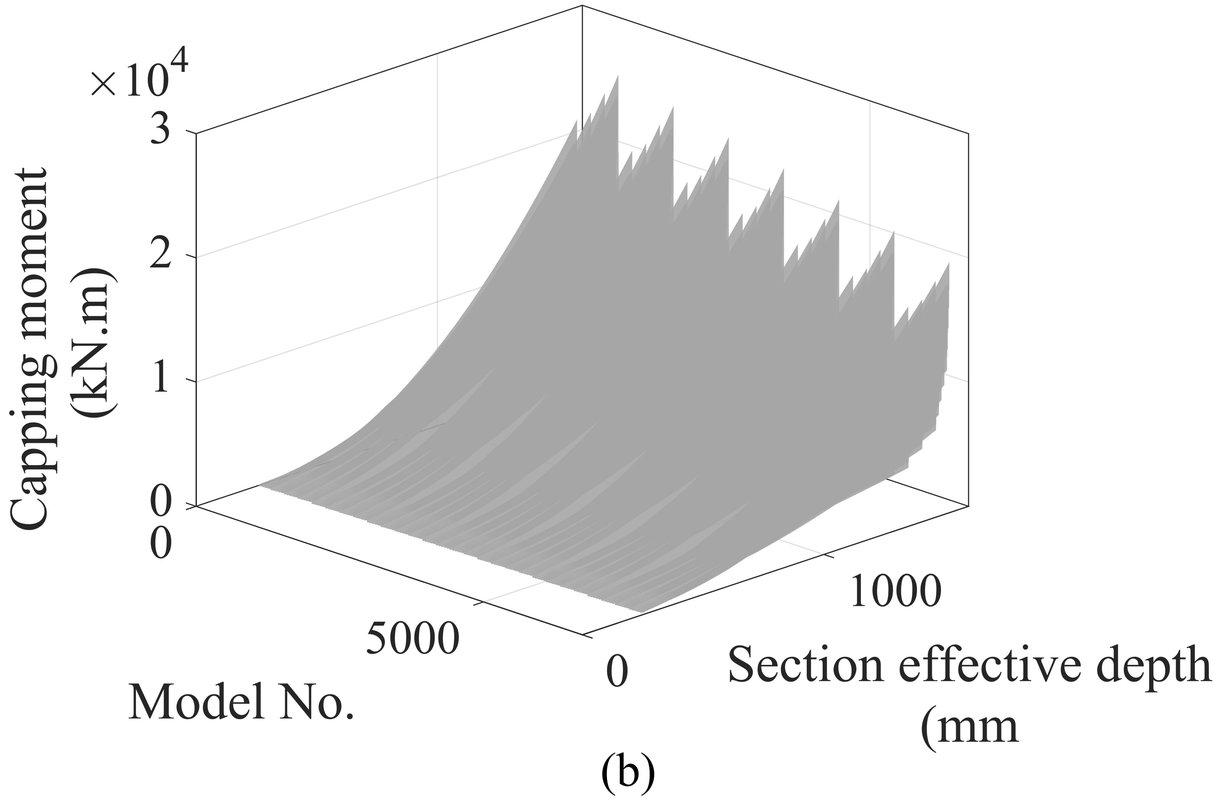
×10^4
3
2
1
0
Capping moment
(kN.m)
0
5000
Model No.
0
1000
Section effective depth
(mm

(b)

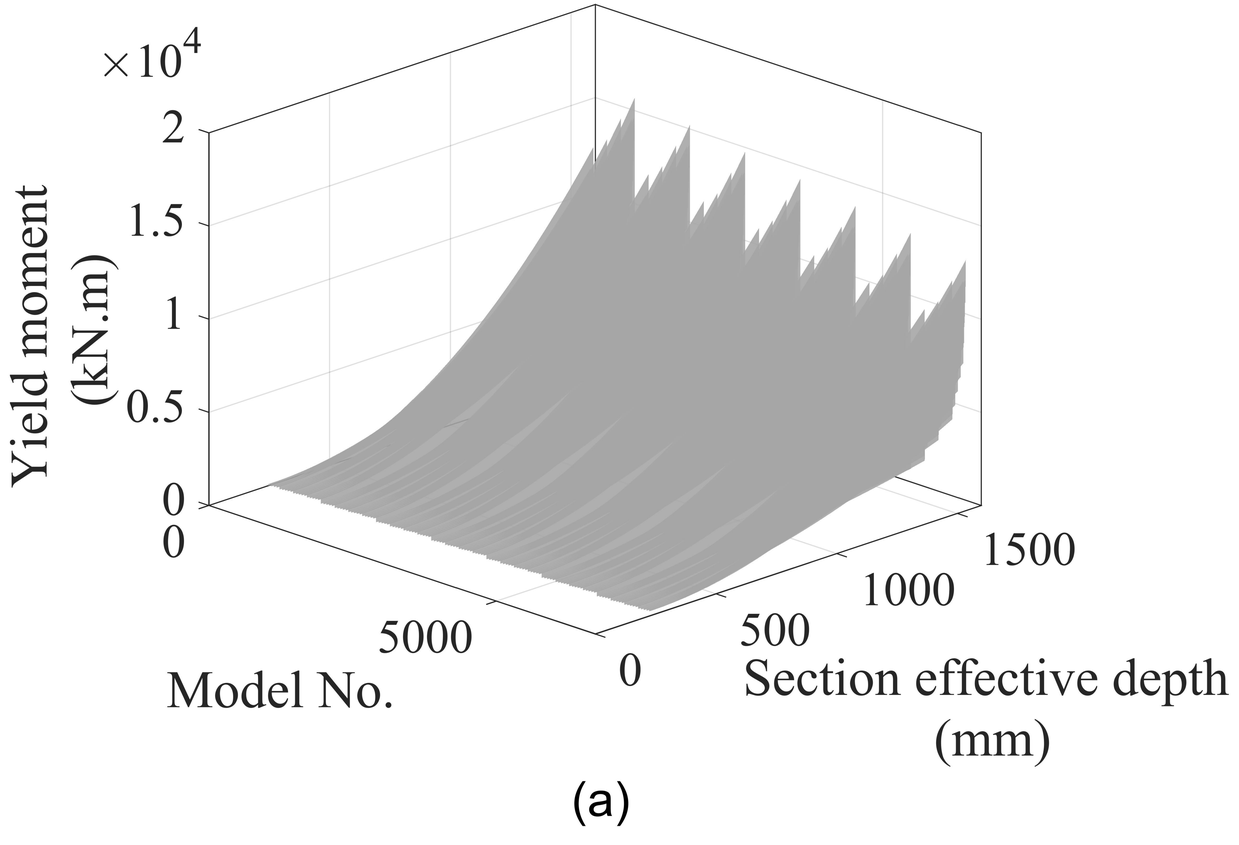
×10^4
2
1.5
1
0.5
0
Yield moment
(kN.m)
0
5000
Model No.
0
500
1000
1500
Section effective depth
(mm)

(a)

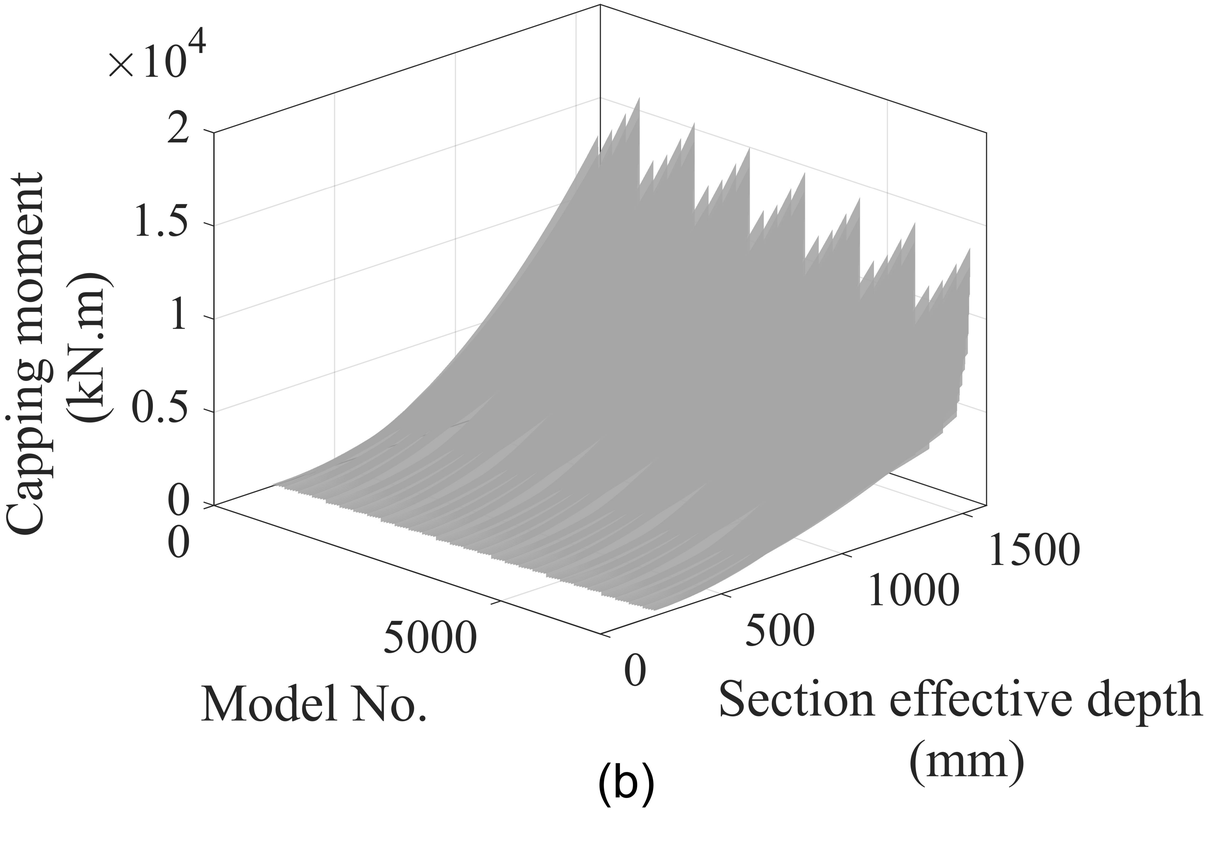
×10^4
2
1.5
1
0.5
0
Capping moment
(kN.m)
0
5000
Model No.
0
500
1000
1500
Section effective depth
(mm)

(b)

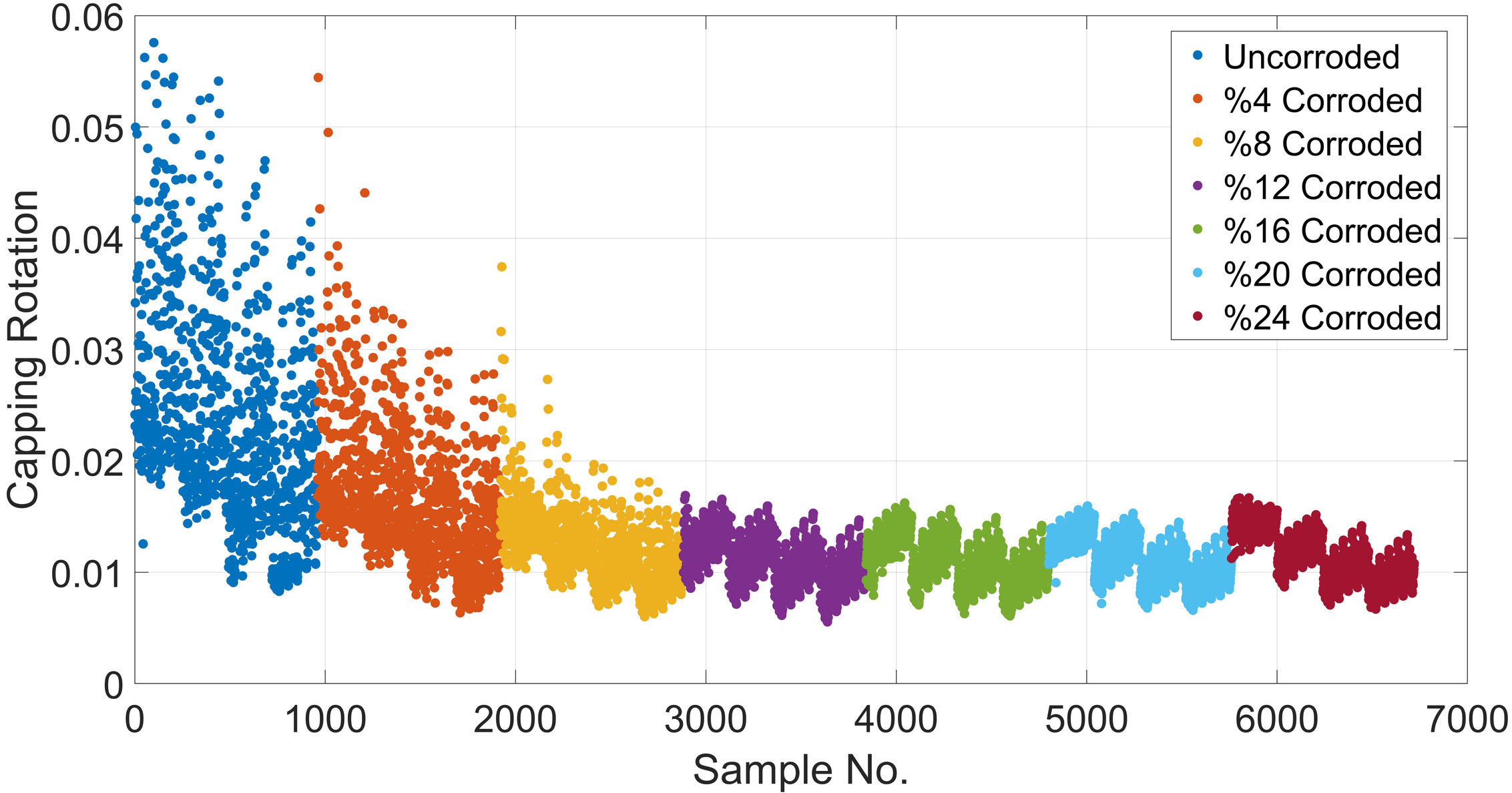
Capping Rotation
Sample No.
0
0.01
0.02
0.03
0.04
0.05
0.06
0
1000
2000
3000
4000
5000
6000
7000
Uncorroded
%4 Corroded
%8 Corroded
%12 Corroded
%16 Corroded
%20 Corroded
%24 Corroded

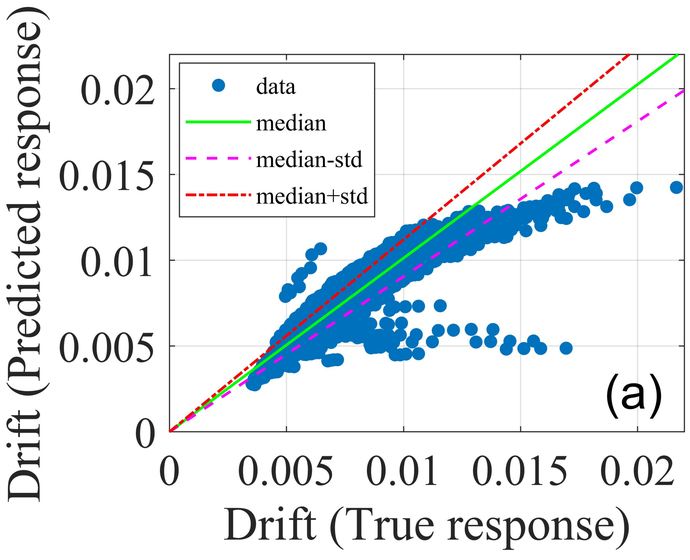
data
median
median-std
median+std
(a)
Drift (Predicted response)
Drift (True response)
0
0.005
0.01
0.015
0.02

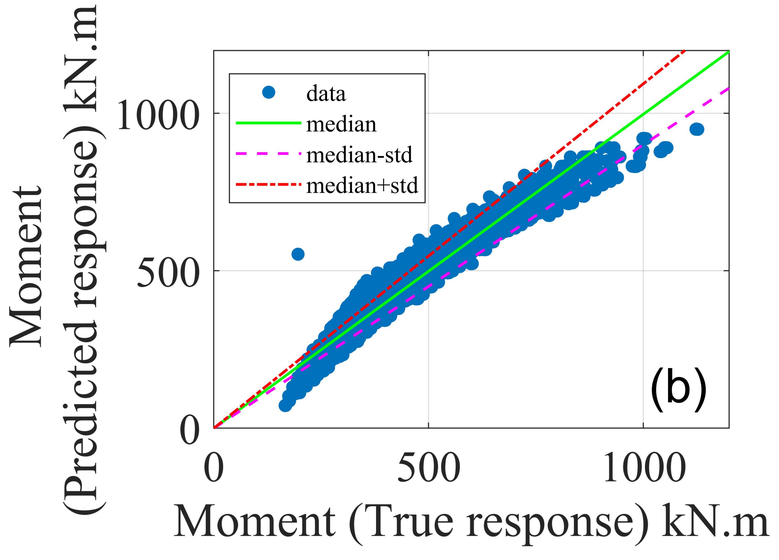
data
median
median-std
median+std
(b)
Moment (Predicted response) kN.m
Moment (True response) kN.m
0
500
1000

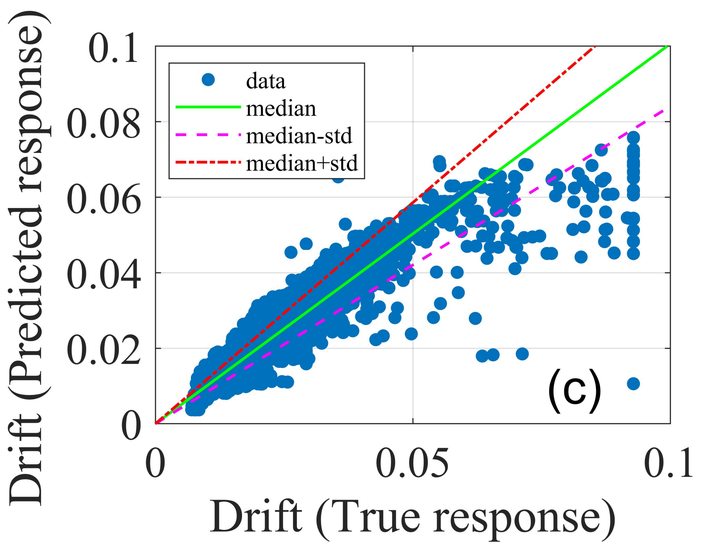
data
median
median-std
median+std
(c)
Drift (Predicted response)
Drift (True response)
0
0.02
0.04
0.06
0.08
0.1

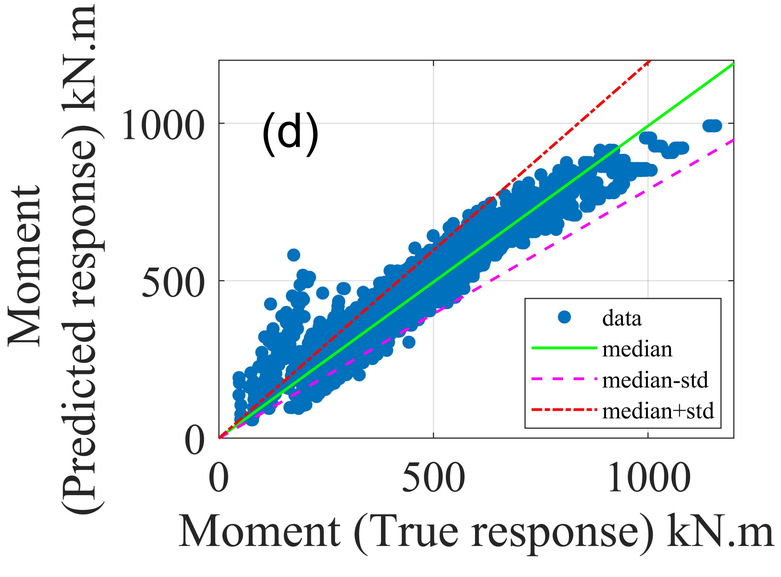
data
median
median-std
median+std
(d)
Moment (Predicted response) kN.m
Moment (True response) kN.m
0
500
1000

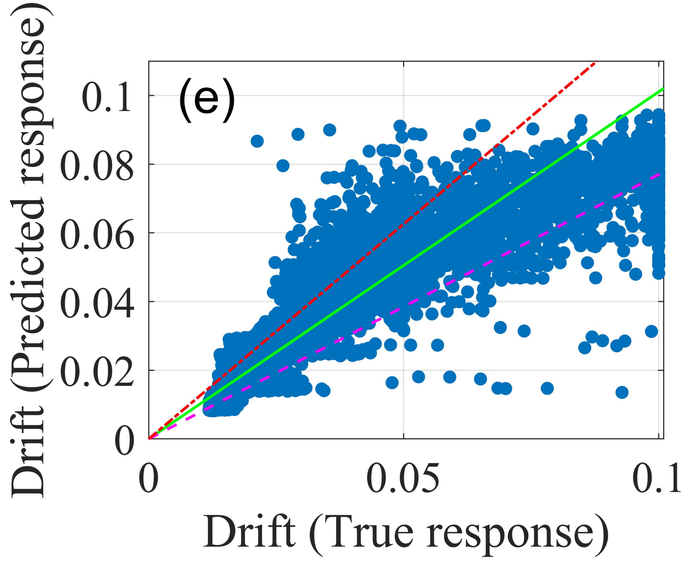
(e)
Drift (Predicted response)
Drift (True response)
0
0.02
0.04
0.06
0.08
0.1

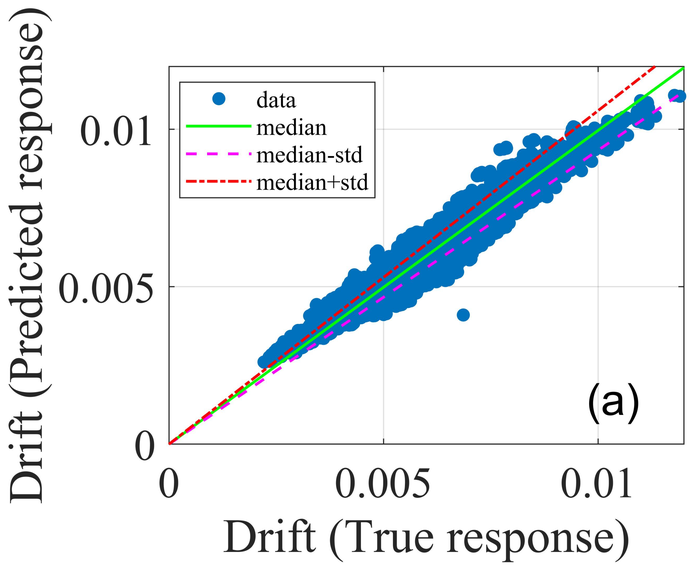
data
median
median-std
median+std
0.01
0.005
0
0
0.005
0.01
Drift (Predicted response)
Drift (True response)
(a)

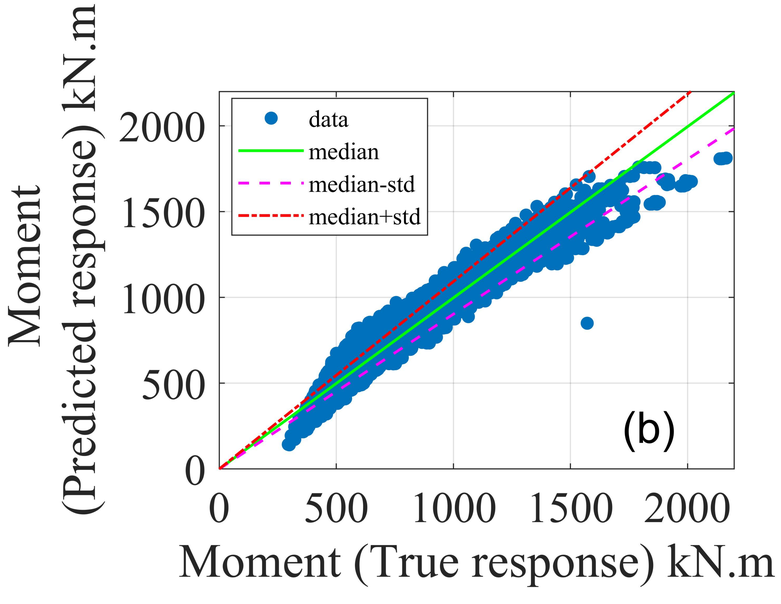
data
median
median-std
median+std
2000
1500
1000
500
0
0
500
1000
1500
2000
Moment (Predicted response) kN.m
Moment (True response) kN.m
(b)

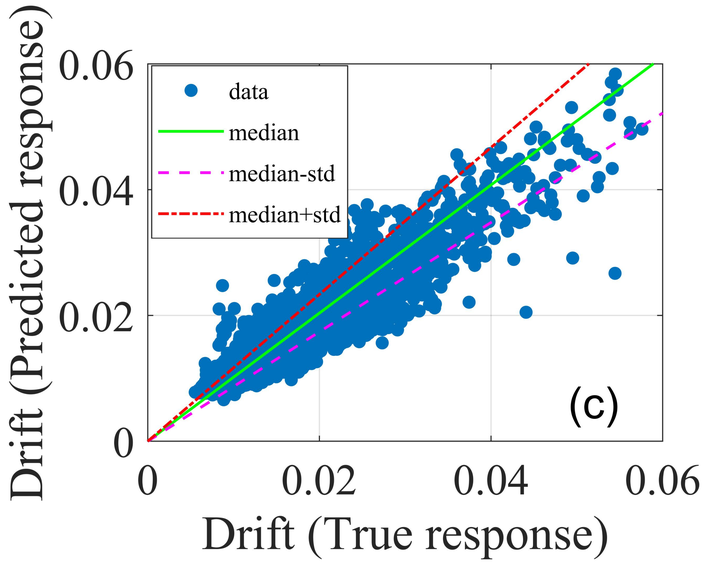
data
median
median-std
median+std
0.06
0.04
0.02
0
0
0.02
0.04
0.06
Drift (Predicted response)
Drift (True response)
(c)

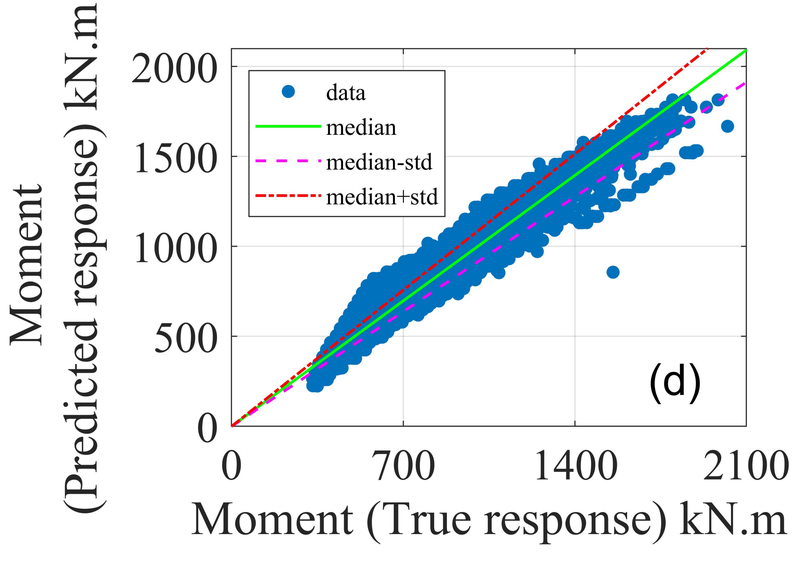
data
median
median-std
median+std
2000
1500
1000
500
0
0
700
1400
2100
Moment (Predicted response) kN.m
Moment (True response) kN.m
(d)

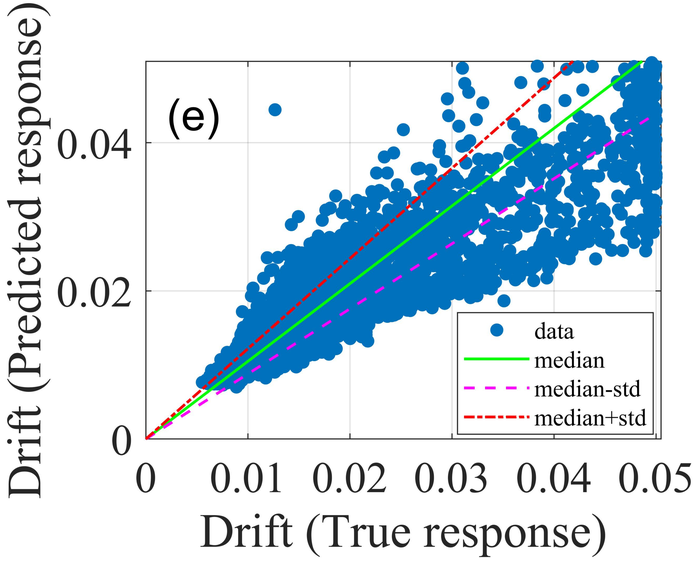
data
median
median-std
median+std
0.04
0.02
0
0
0.01
0.02
0.03
0.04
0.05
Drift (Predicted response)
Drift (True response)
(e)

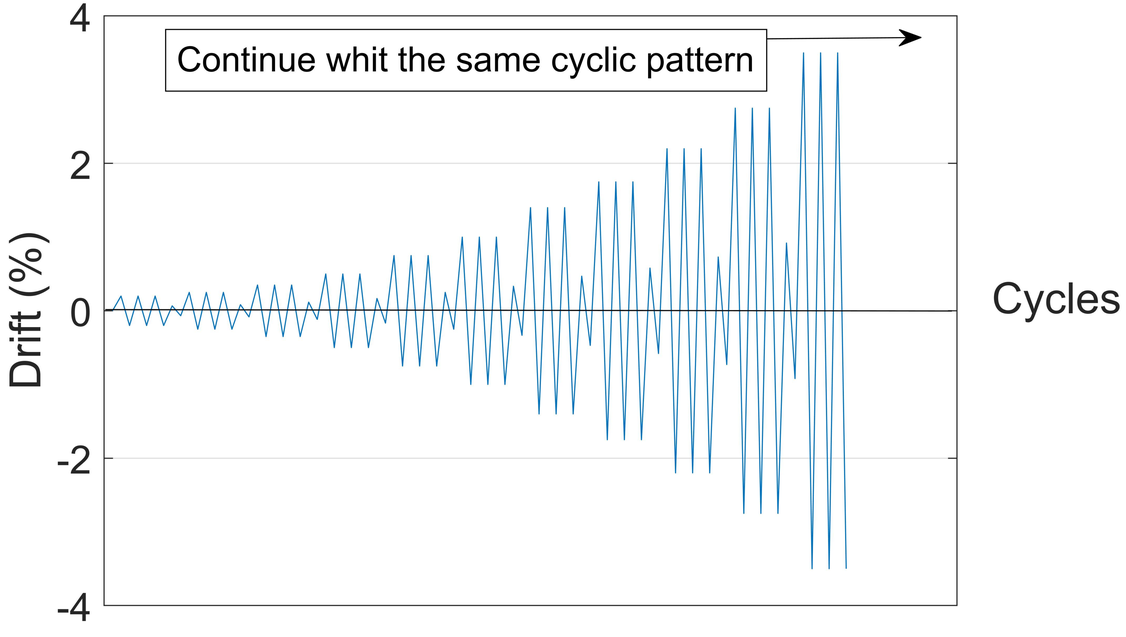
Continue whit the same cyclic pattern
4
2
0
-2
-4
Drift (%)
Cycles

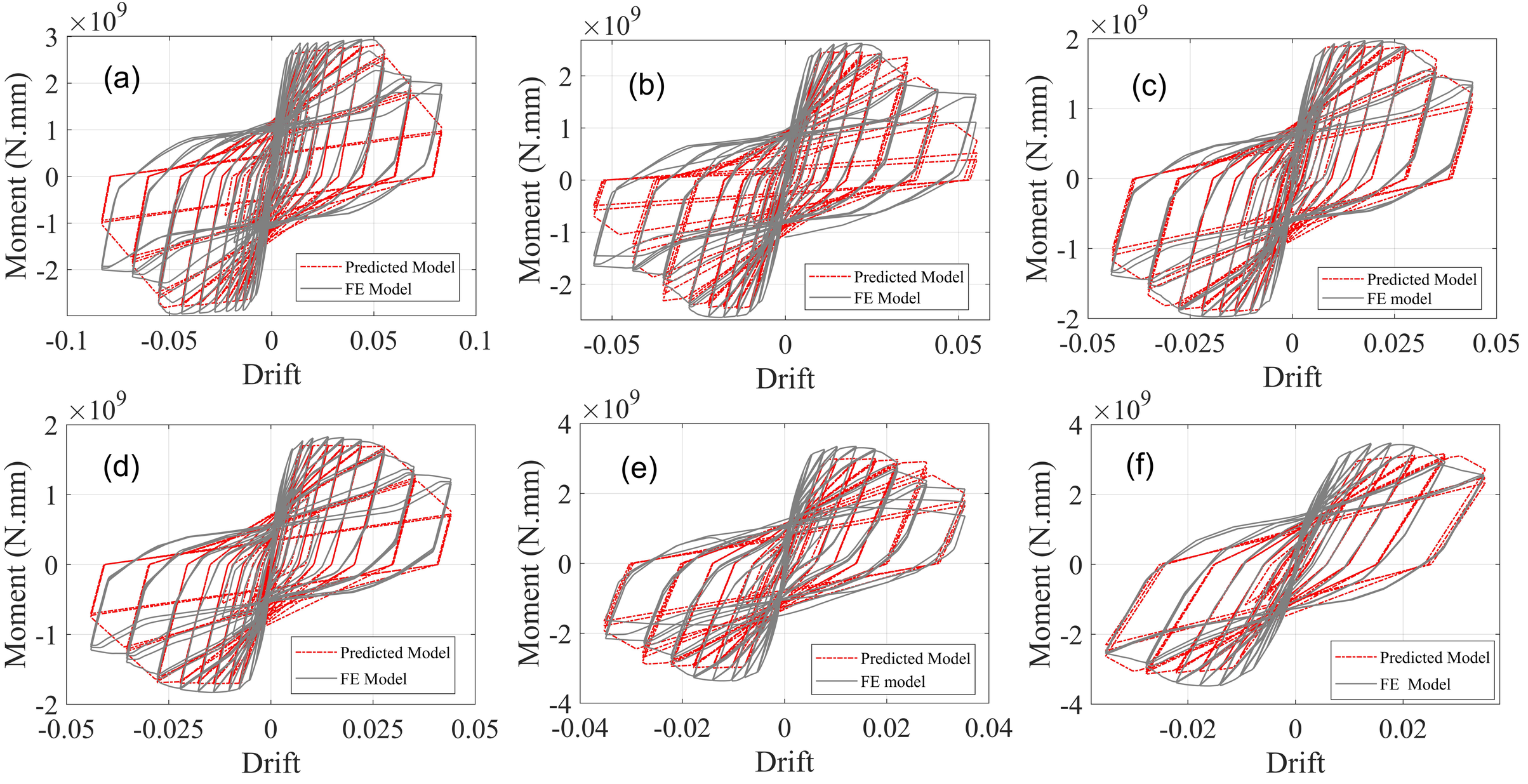
(a)
(b)
(c)
(d)
(e)
(f)
Moment (N.mm)
Drift
×10^9
Predicted Model
FE Model
FE model

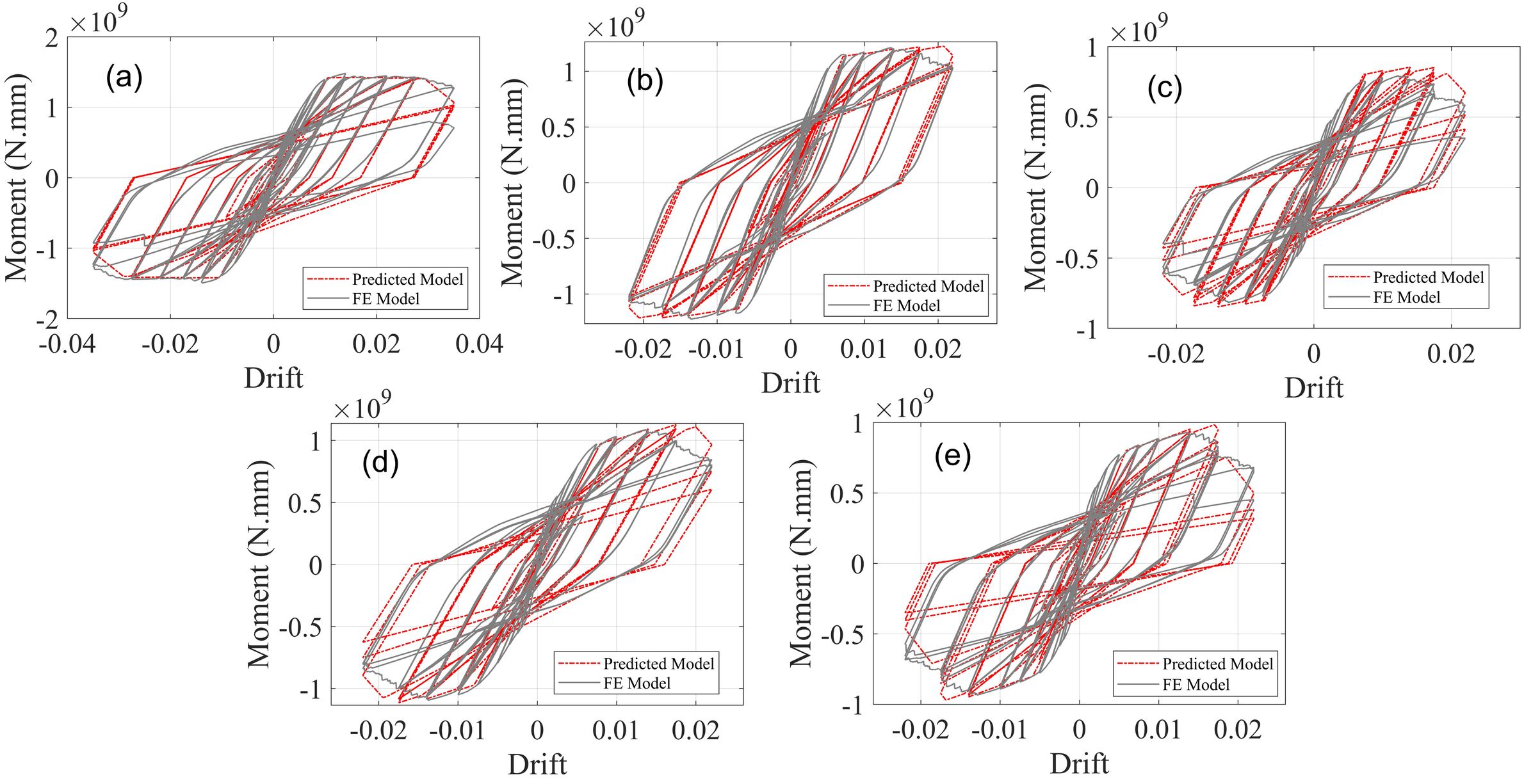
(a)
(b)
(c)
(d)
(e)
Moment (N.mm)
Drift
×10^9
Predicted Model
FE Model

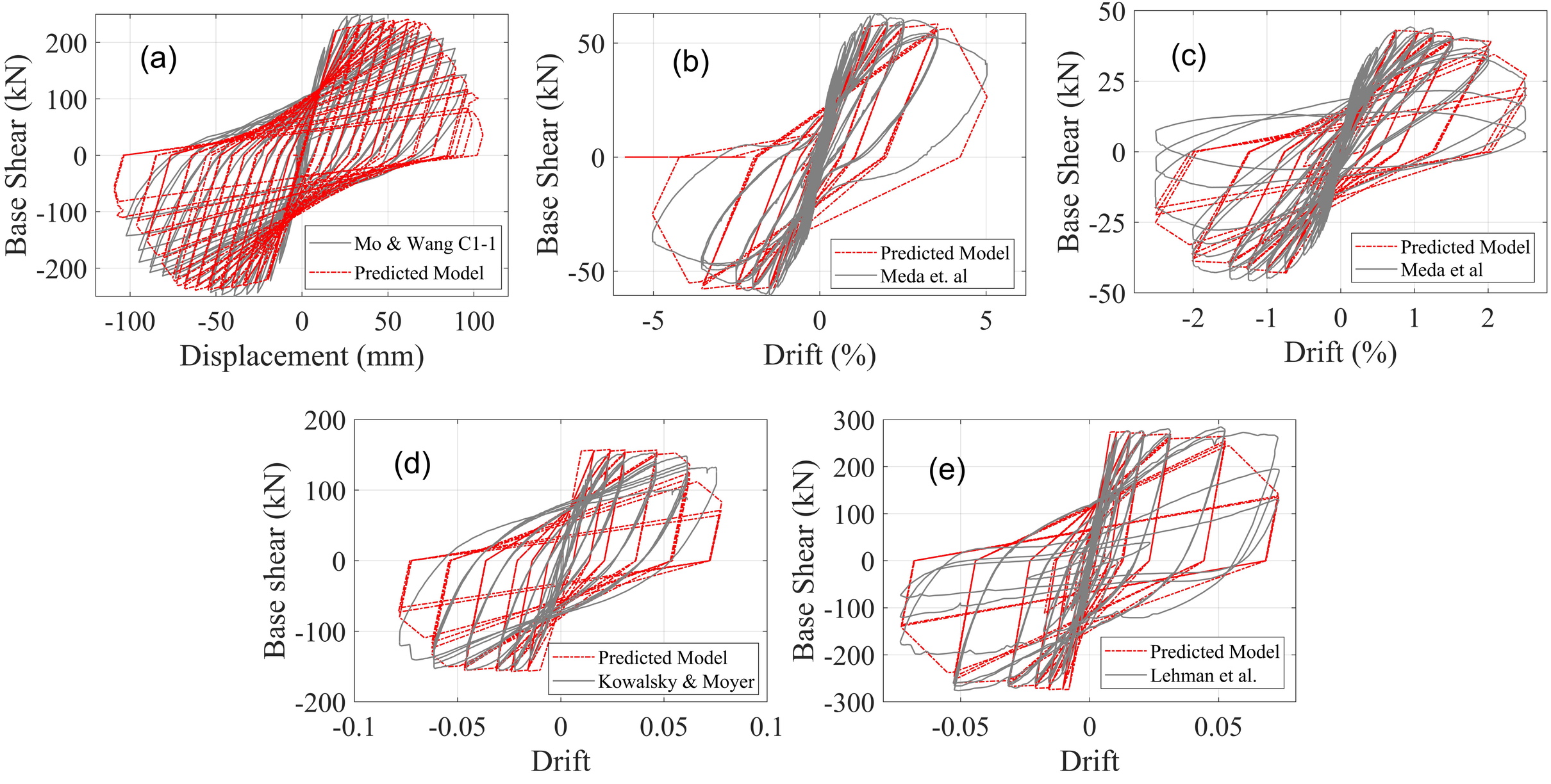
(a)
Base Shear (kN)
Displacement (mm)
Mo & Wang C1-1
Predicted Model
(b)
Base Shear (kN)
Drift (%)
Predicted Model
Meda et. al
(c)
Base Shear (kN)
Drift (%)
Predicted Model
Meda et al
(d)
Base shear (kN)
Drift
Predicted Model
Kowalsky & Moyer
(e)
Base Shear (kN)
Drift
Predicted Model
Lehman et al.

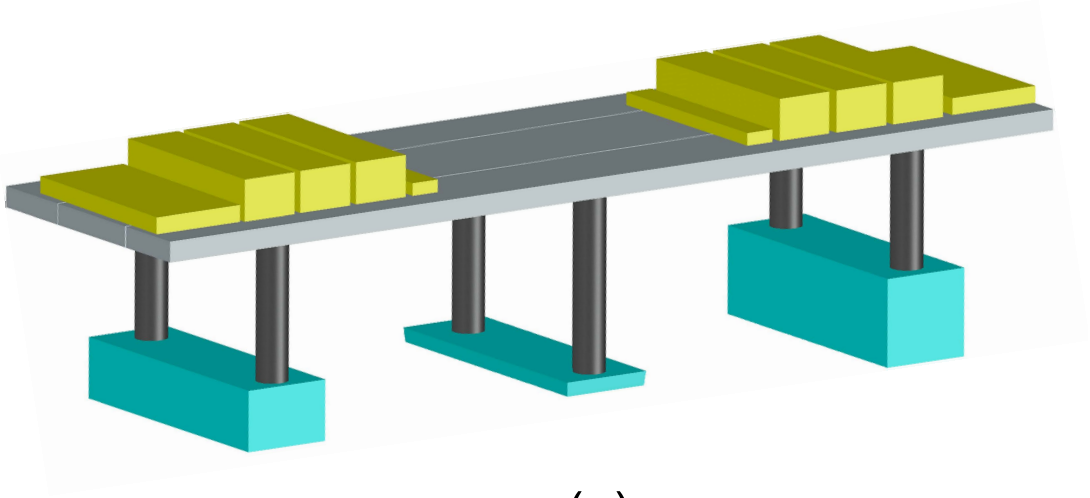

(a)

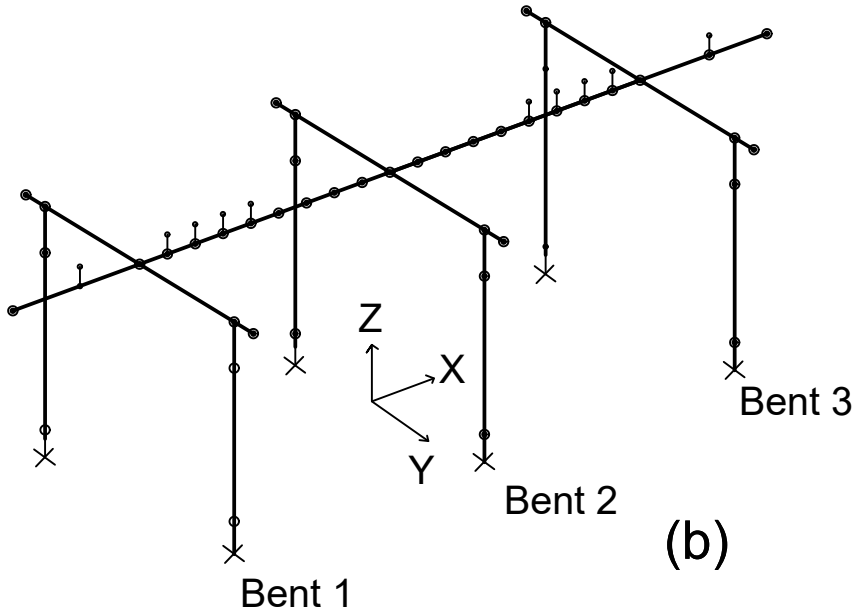

(b)

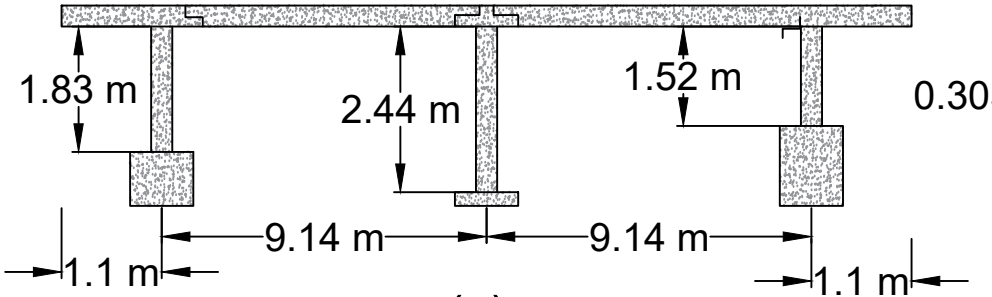

(c)

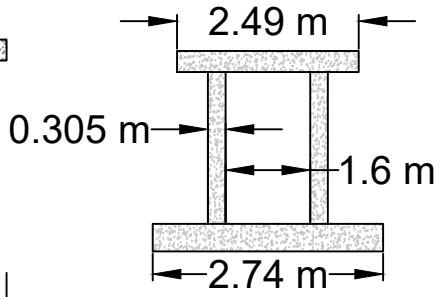

(d)

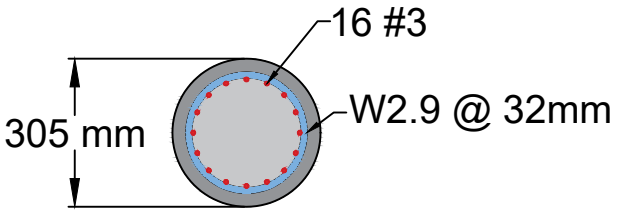

(e)

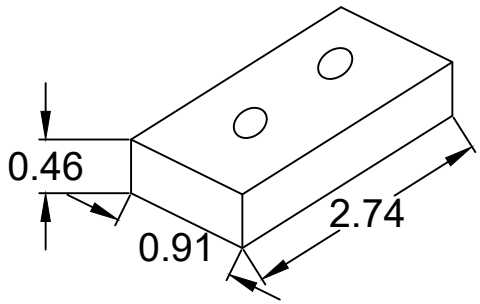

Bent 1 & 2

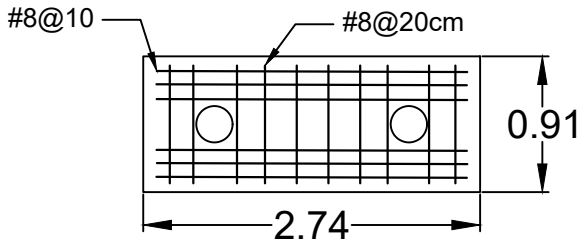

Bent 1,2 & 3

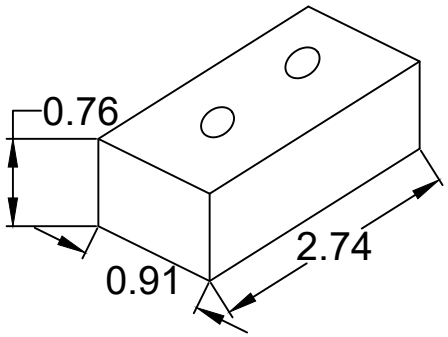

Bent 3

(f)

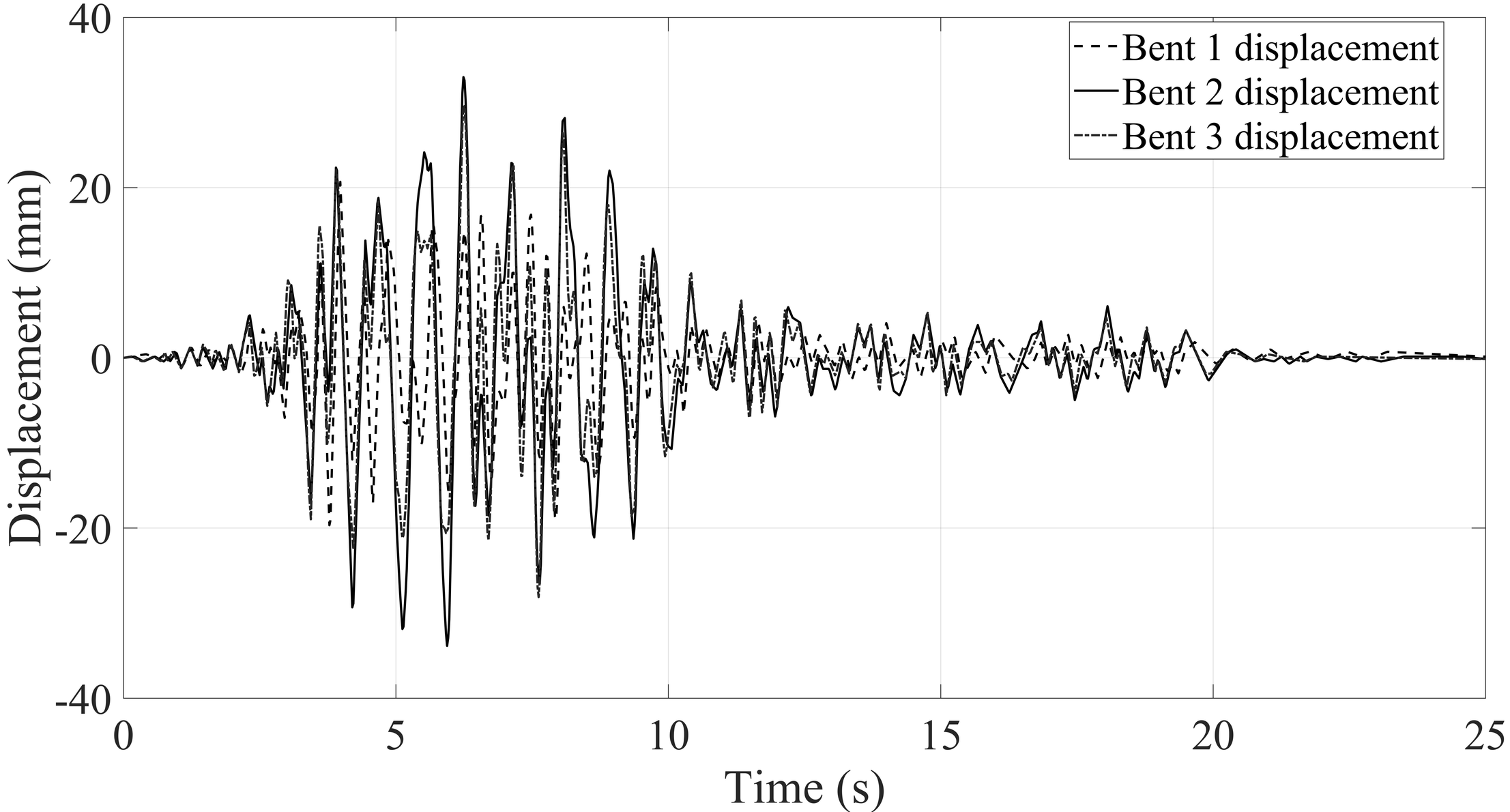
Bent 1 displacement
Bent 2 displacement
Bent 3 displacement
Displacement (mm)
40
20
0
-20
-40
0
5
10
15
20
25
Time (s)

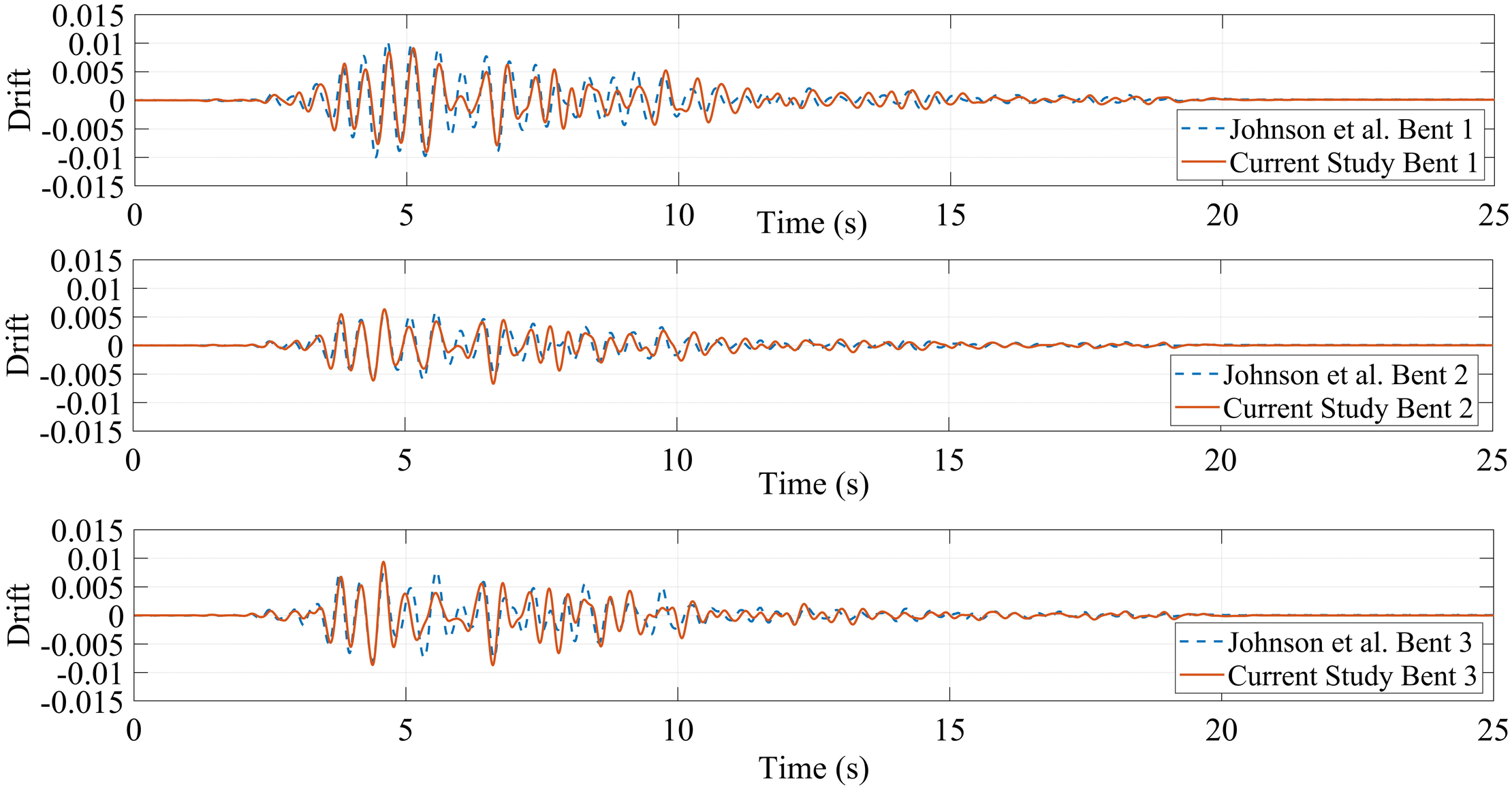
Drift
0.015
0.01
0.005
0
-0.005
-0.01
-0.015
0
5
10
15
20
25
Time (s)
Johnson et al. Bent 1
Current Study Bent 1
Drift
0.015
0.01
0.005
0
-0.005
-0.01
-0.015
0
5
10
15
20
25
Time (s)
Johnson et al. Bent 2
Current Study Bent 2
Drift
0.015
0.01
0.005
0
-0.005
-0.01
-0.015
0
5
10
15
20
25
Time (s)
Johnson et al. Bent 3
Current Study Bent 3

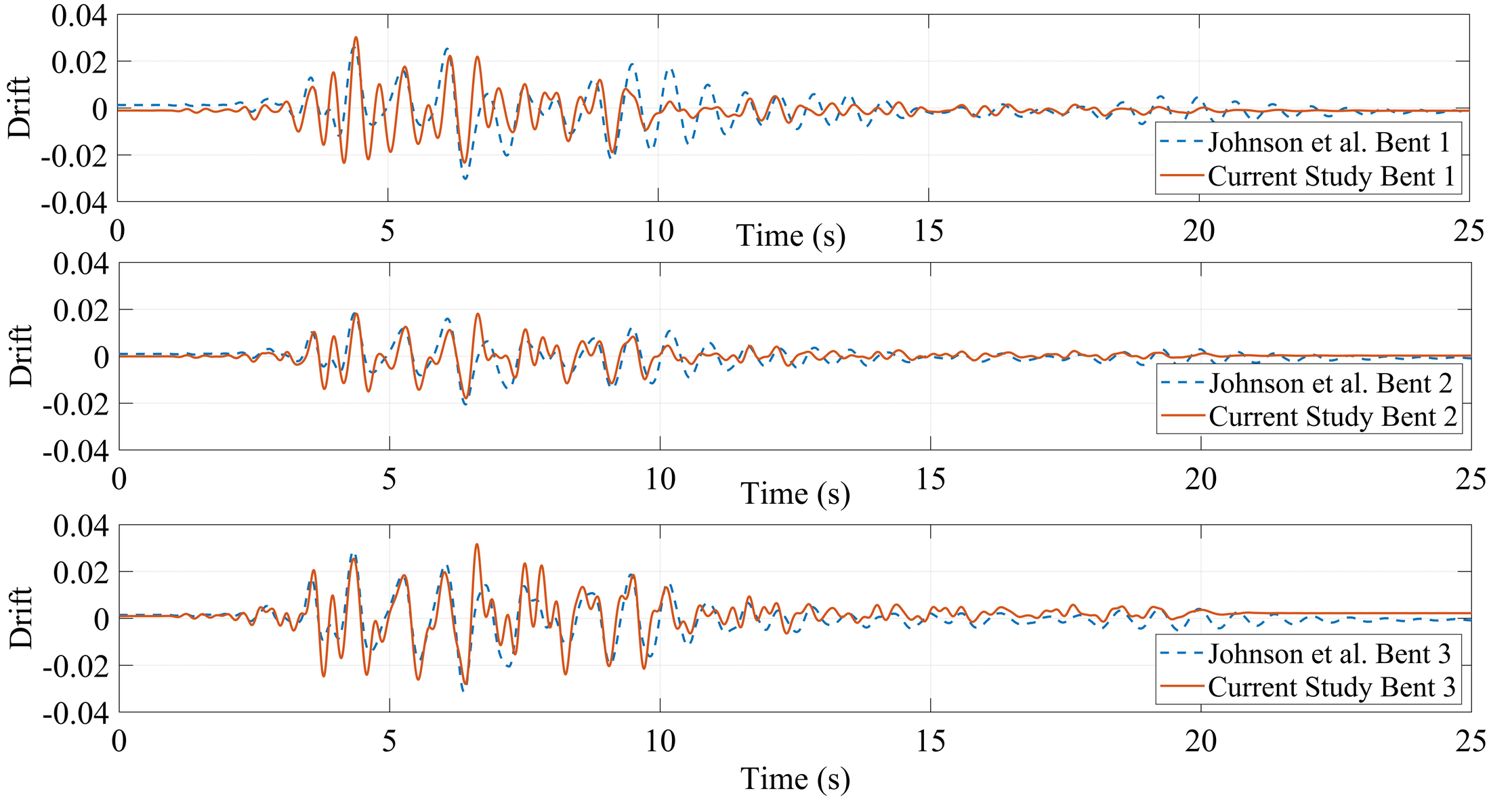
0.04
0.02
0
-0.02
-0.04
Drift
0
5
10
15
20
25
Time (s)
Johnson et al. Bent 1
Current Study Bent 1
Johnson et al. Bent 2
Current Study Bent 2
Johnson et al. Bent 3
Current Study Bent 3

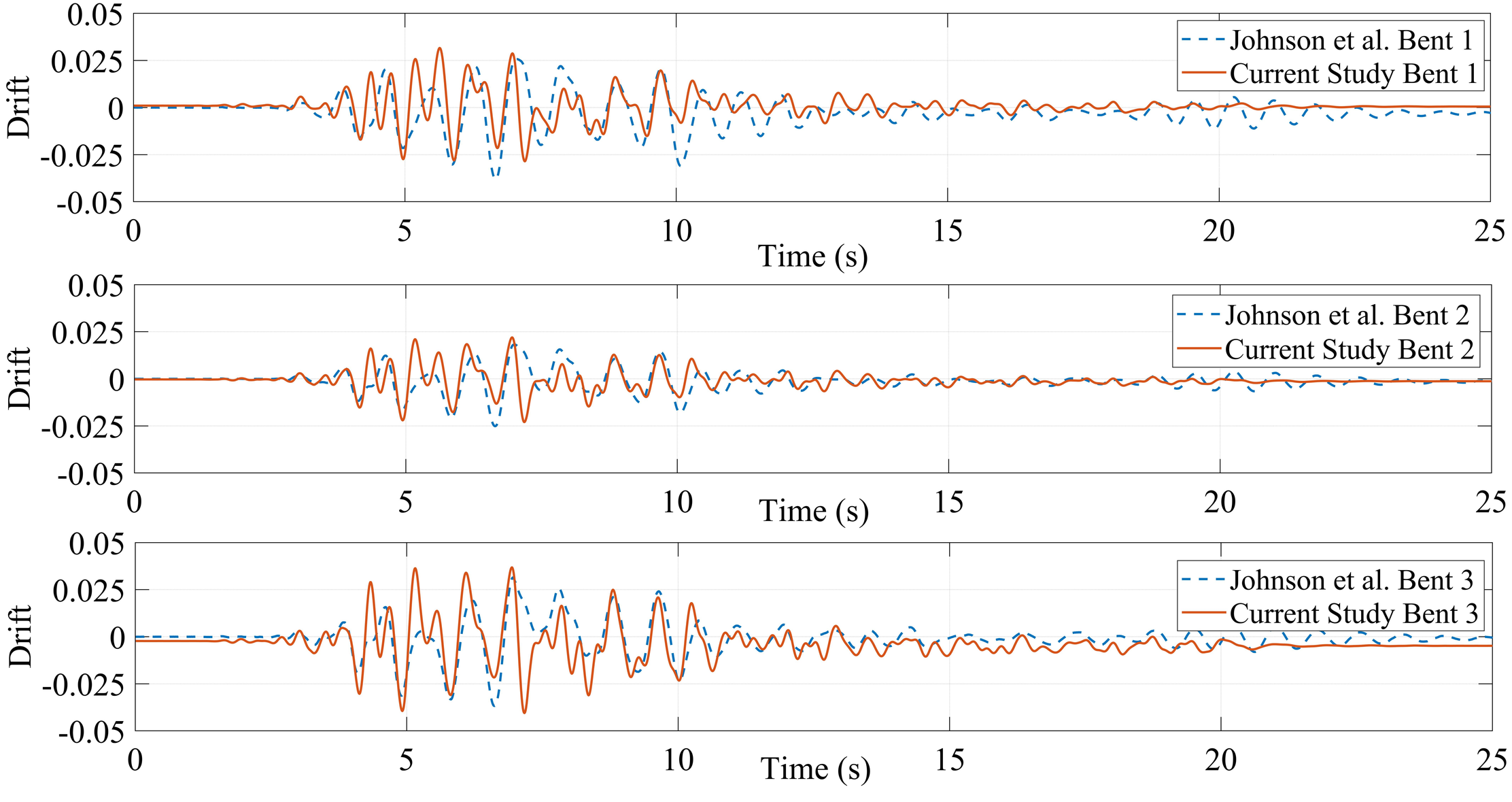
Drift
0.05
0.025
0
-0.025
-0.05
0
5
10
15
20
25
Time (s)
Johnson et al. Bent 1
Current Study Bent 1
Johnson et al. Bent 2
Current Study Bent 2
Johnson et al. Bent 3
Current Study Bent 3